comprising SOD1 and chromogranins (**Fig. 4**; CgA bottom left, CgB bottom right). This colocalization was observed in rough ER, transport vesicles and granule-like structures. In contrast, wild-type SOD1 was chiefly located in the cytosol and occasionally in mitochondria and luminal structures including smooth and rough ER. The gold particles for wild-type human SOD1 tended to be singular or doublets, whereas clusters for G37R SOD comprised five to ten gold particles (**Supplementary Fig. 3**). No significant colocalization of wild-type SOD1 and chromogranins was detected. These findings confirm that mutant SOD1 can be recruited into the ER-Golgi pathway and interact with chromogranins.

Expression of CgA in reactive astrocytes in ALS mice

CgA is implicated in several neurodegenerative diseases including Alzheimer disease[21] and prion disease[22]. The N-terminal bioactive peptide of CgA, vasostatin, is implicated in microglial activation[24,32]. To investigate the distribution of proinflammatory fragments of CgA in the mutant *SOD1* transgenic mice, we raised a rabbit polyclonal antibody specific to the N-terminal peptide (16 amino acids) of the mature mouse CgA (anti-mCgA-N′).

Western analysis showed that anti-mCgA-N′ specifically recognized mouse CgA tagged by HA in the transfected COS-7 cells. Moreover, this antibody reacts with mouse CgA, but not with human CgA (**Supplementary Fig. 4** online). In transgenic mice overexpressing wild-type SOD1 (9 months old), immunofluorescence using anti-mCgA-N′ showed CgA detection predominantly in neurons co-stained with anti-NeuN (**Fig. 5a**) and rarely in astrocytes labeled by antibody specific to glial fibrillary acidic protein (anti-GFAP; **Fig. 5b**). In contrast, prominent anti-mCgA-N′ immunoreactivity was observed in reactive astrocytes of ventral horn in presymptomatic G37R *SOD1* mice (**Fig. 5c–e**, 8 months old) and G93A *SOD1* mice (**Supplementary Fig. 5** online, 80 d old). CgA also localized in neurons (**Fig. 5c**) but not in Mac2-labeled microglia (**Fig. 5e**) of G37R *SOD1* mice. Pre-incubation with the peptide antigen completely eliminated the signal (data not shown). These results suggest that CgA may be involved in the disease progression concomitant with astrocytosis.

CgA and CgB promote secretion of mutant SOD1

The combined microscopy and immunoprecipitation data presented above provide compelling evidence for the selective colocalization of

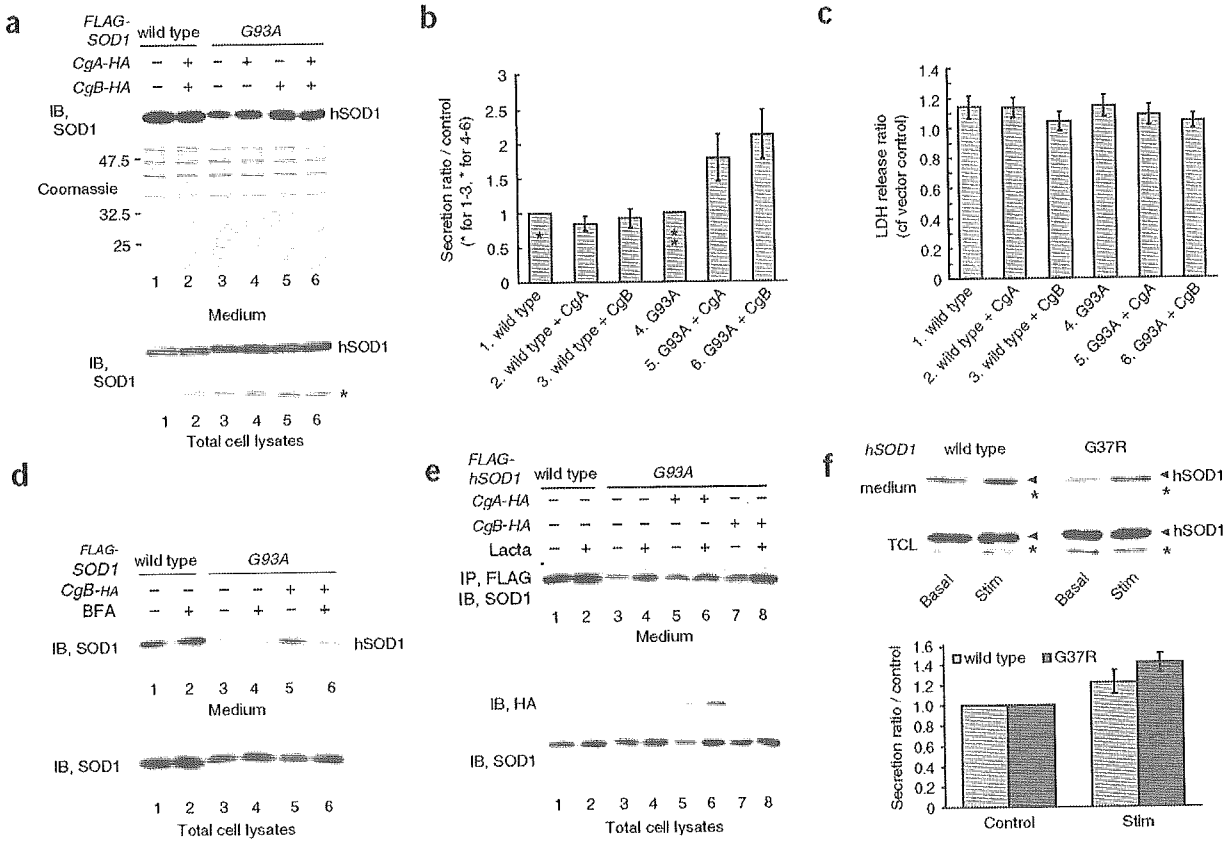

Figure 6 Chromogranins promote selective secretion of misfolded mutant SOD1. (**a**) CgA and CgB promoted specific secretion of mutant SOD1 in non-neurosecretory cells. COS-7 cells transfected with *FLAG-SOD1* (wild-type or G93A) and *CgA-HA* or *CgB-HA* were incubated in stimulation buffer. Medium was concentrated and analyzed by western blotting using SOD1-specific antibody. The SDS-PAGE gel was stained by Coomassie brilliant blue (Coomassie). Asterisk indicates endogenous SOD1. IB, immunoblot. (**b**) Densitometry of the secreted human SOD1 from the western blots. The values (mean ± s.e.m., $n = 3$) represent the ratio compared to control (lane 1 = control for wild-type (asterisk) and lane 4 = control for G93A SOD1 (double asterisks)). (**c**) LDH release assay demonstrating that transfection experiments did not provoke cell leakage. Medium was assayed 24 h after transfection. Value represents LDH release ratio compared with vector control (*pcDNA3*). Data are mean ± s.e.m. ($n = 3$). (**d**) Brefeldin A (BFA) inhibited chromogranin-mediated secretion of mutant SOD1. COS-7 cells transfected with FLAG-*SOD1* (wild-type or G93A) with or without CgB-HA were treated with 5 μM BFA for 1 h before exposure to stimulation buffer. (**e**) Effect of proteasomal inhibitor on mutant SOD1 secretion. Transfected NIH3T3 cells were treated with lactacystin for 20 h before the secretion assay. (**f**) Both wild-type and G37R SOD1 were secreted from embryonic spinal cord cultures from human SOD1 transgenic mice. Primary cultures were treated with basal or stimulation buffer for 15 min. Asterisks indicate endogenous mouse SOD1. Data given as ratio of secreted SOD1 from treated samples to that in basal-buffer samples (mean ± s.e.m., $n = 4$).

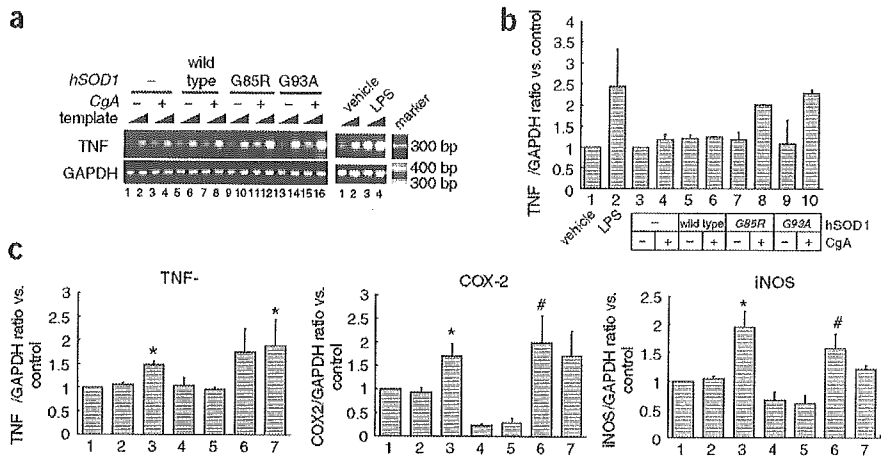

Figure 7 Activation of microglia by extracellular mutant SOD1. (**a**,**b**) Activation of microglial cell-line BV2 after treatment with conditioned medium from Neuro2a cells co-transfected with CgA and *SOD1* mutants (G85R or G93A). (**a**) RT-PCR study of TNF-α and GAPDH. For control, Neuro2a cells were treated with lipopolysaccharide (LPS). Notably, there was no microglial activation with medium from cells co-transfected with *CgA* and wild-type *SOD1*. Templates were examined at two different concentrations (1:10 diluted and original). (**b**) Each densitometric value was normalized with GAPDH and averaged from results of two different concentrations of templates. Each value represents a ratio compared to control lanes (bar 1 is the control for bar 2, and bar 3 is the control for 4–10), expressed as mean ± s.e.m. (**c**) Direct effect of mutant SOD1 on microglial activation. BV2 cells were treated with recombinant CgA (1 μg ml $^{-1}$), human SOD1 (wild-type or G93A, 2 μg ml $^{-1}$ each) or LPS (10 μg ml $^{-1}$) as a positive control for 18 h, as shown in the bottom box. Semi-quantitative RT-PCR was performed in the same manner as in **a**. Each densitometric value was normalized by GAPDH and an expression ratio was obtained by comparison with control (bar 1 in each graph). The ratio was averaged from three experiments and expressed as mean ± s.e.m. $^{*}P < 0.05$ versus sham treatment (lane 1). $^{\#}P < 0.05$ versus wild-type SOD1 treatment (lane 4) assessed by analysis of variance (ANOVA).

mutant SOD1 with chromogranins in mouse models of ALS. These results prompted us to investigate whether mutant SOD1 molecules were secreted together with chromogranins. We conducted secretion experiments using nongranular COS-7 cells that are lacking endogenous chromogranins[33]. Expression plasmids coding for FLAG-tagged SOD1 (wild-type or G93A mutant) and HA-tagged mouse CgA or CgB were transiently co-transfected in COS-7 cells. Both wild-type and G93A mutant SOD1 were detected by western analysis in the control medium after a 15-min incubation. Moreover, treatment with stimulation buffer containing 2-mM $BaCl_2$ and 50 mM KCl increased the amount of both wild-type and mutant SOD1 in the medium 1.2-fold compared with control buffer (data not shown). These data imply the existence of constitutive and regulatory secretory pathways for SOD1 in these cells. It is noteworthy that both CgA and CgB promoted secretion of G93A SOD1, whereas secretion of wild-type SOD1 was not affected by CgA or CgB (**Fig. 6a,b**). Judging from the amount of lactate dehydrogenase (LDH) released, the effects of chromogranins on secretion of mutant SOD1 did not result from cell death or membrane disintegration caused by overexpression (**Fig. 6c**). We also examined the effect of Brefeldin A (BFA) on SOD1 secretion to further address the involvement of the ER-Golgi network. In COS-7 cells, BFA did not reduce the secretion of either mutant or wild-type SOD1 in absence of CgB (**Fig. 6d**, lanes 2 and 5). BFA did, however, inhibit the CgB-mediated secretion of mutant SOD1 (**Fig. 6d**, lanes 7 and 8). This suggests that CgB contributes to the secretion of mutant SOD1 proteins through the TGN. We conclude that chromogranins promote the secretion of mutant SOD1, but not of wild-type SOD1.

Proteasome inhibition enhances secretion of mutant SOD1

Because previous studies showed an impairment of proteasomal activity in cells expressing mutant SOD1[11], we examined the effect of a proteasome inhibitor on the secretion of human SOD1 species in non-granular NIH3T3 cells. The treatment of transfected NIH3T3 cells with a specific proteasome inhibitor, lactacystin (5 μM), enhanced the secretion of mutant SOD1 in the presence or absence of chromogranins (**Fig. 6e**).

SOD1 secretion from spinal cultures of SOD1 mouse embryo

Both wild-type and mutant SOD1 have been detected in the cerebrospinal fluid (CSF) of *SOD1* transgenic rats[34] and humans carrying a SOD1 mutation[35]. However, it is technically difficult to prove this finding in mice, because of the small space for CSF with high occurrence of contamination from the blood or tissues. We carried out spinal cord cultures from *SOD1* transgenic mice to confirm that SOD1 can be secreted. Spinal cord cultures were prepared from E13 embryos and then analyzed after 14 d *in vitro*. Secretion analysis of the culture medium revealed that both wild-type and G37R SOD1 can be detected in basal secretion buffer. Exposure of the cells to stimulation buffer containing $BaCl_2$ (2 mM) and KCl (50 mM) for 15 min promoted the secretion of both wild-type and G37R SOD1, but more robustly in G37R (**Fig. 6f**). This result indicates that SOD1 can be secreted in both a constitutive and regulated manner.

Extracellular SOD1 mutants cause microgliosis and neuron death

There is evidence for involvement of CgA in microglial activation[32]. To examine the effects of secreted mutant SOD1 together with CgA on microglial activation, we treated BV2 microglial cells with conditioned medium from Neuro2a cells that were transfected with various human *SOD1* species (wild-type, G85R and G93A), with or without CgA. Semi-quantitative reverse-transcriptase PCR (RT-PCR) was performed using total RNA from BV2 cells to monitor expression of mRNA for proinflammatory molecules. RT-PCR results showed that the combination of mutant SOD1 and CgA resulted in a medium that induced TNF-α expression in BV2 cells (**Fig. 7a,b**).

To investigate whether extracellular SOD1 mutants activate microglia, we exposed the BV2 cells to recombinant human SOD1 or CgA (extracellular) to determine whether microglial activation was mediated directly by these molecules. The results showed that extracellular mutant G93A SOD1 with or without CgA induced BV2 cells to produce TNF-α, cyclooxygenase-2 (COX-2) and inducible nitric oxide synthase (iNOS) (**Fig. 7c**). In contrast to mutant SOD1, the recombinant wild-type SOD1 caused suppression of microglial activation, which is in agreement with a protective role for secreted wild-type SOD1 as recently suggested[35].

We further investigated the effects of extracellular SOD1 (wild-type and G93A) and CgA proteins using primary spinal cord cultures derived from E13 mouse embryos. Spinal cord cultures at 14 d after plating were exposed to these recombinant proteins or to lipopolysaccharide (LPS) for 24 h. Treatment of the cultures with CgA and/or

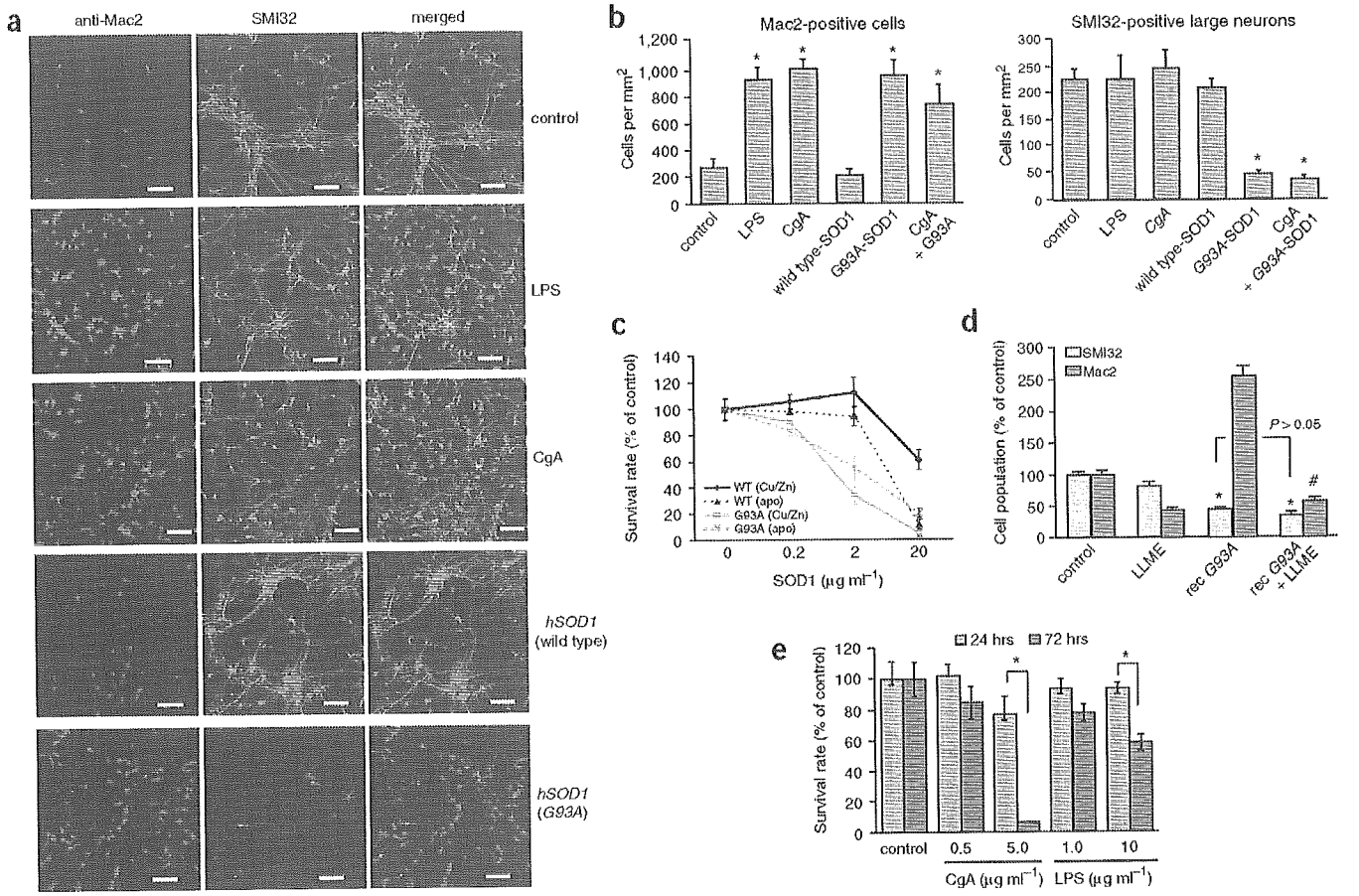

Figure 8 Extracellular SOD1 mutant triggers microgliosis and motor neuron death. **(a)** Immunofluorescence images of primary spinal cultures doubly stained by anti-Mac2 antibody and SMI32. Scale bars, 50 μm. **(b)** Extracellular SOD1 mutant activated microglia and killed motor neurons of embryonic spinal cord cultures. Spinal cord cultures were treated with lipopolysaccharide (LPS, 10 μg ml $^{-1}$), recombinant mouse CgA (5 μg ml $^{-1}$) or recombinant SOD1 (wild-type or G93A, 2 μg ml $^{-1}$) for 24 h. Cultures were fixed with 4% paraformaldehyde and doubly labeled with antibody to Mac2 (top) or antibody to the nonphosphorylated neurofilament NFH (SMI32) (bottom). The number of labeled cells at eight different areas from two sister cultures were averaged and expressed as cells per mm^2. Values indicate mean ± s.e.m. ($n = 8$). *$P < 0.01$ versus controls. **(c)** Dose-dependent toxicity of G93A and wild-type SOD1 in holo- or apo-states to spinal cord cultures. Spinal cultures were exposed to metal-deficient (apo) or metallated (Cu/Zn) recombinant G93A SOD1 or wild-type SOD1 for 24 h. Values indicate mean ± s.e.m. ($n = 8$). **(d)** Elimination of microglia did not affect extracellular SOD1-induced motor neuron death. Cultures were pre-treated with LLME (5 mM) for 16 h before application of recombinant G93A SOD1 (2 μg ml $^{-1}$) for 24 h. Values indicate percent survival compared with control culture (mean ± s.e.m., $n = 8$–24). *$P < 0.01$ versus control, #$P < 0.01$ versus recombinant G93A treatment. **(e)** Motor neuron death caused by longer time exposure to CgA. Spinal cultures were exposed to CgA or LPS for 72 h or 24 h. Values indicate mean ± s.e.m. ($n = 8$). *$P < 0.01$.

G93A SOD1 significantly increased the number of active microglia, like LPS treatment, as determined with antibody specific to Mac2 (**Fig. 8a** and top graph in **Fig. 8b**). On the other hand, whereas exposure to extracellular CgA (5 μg ml $^{-1}$) or LPS (10 μg ml $^{-1}$) for 24 h did not affect the number of motor neurons stained with SMI32 (an antibody that labels unphosphorylated neurofilament-H), recombinant SOD1 mutant (2 μg ml $^{-1}$) caused massive neuronal death (bottom row in **Fig. 8a** and bottom graph in **Fig. 8b**). Thus, both CgA and mutant SOD1 were capable of activating microglia, but only mutant SOD1 was neurotoxic after a 24-h exposure. This toxicity is not related to the metal content, as the apo G93A mutant also exhibited toxicity to motor neurons (**Fig. 8c**). Notably, the apo form of wild-type SOD1 acquired some toxicity at 20 μg ml $^{-1}$ when compared to holo-state wild-type SOD1 (**Fig. 8c**). Furthermore, we investigated the role of microglia in extracellular mutant SOD1–induced motor neuron death by eliminating microglia with exposure to leu-leu methyl ester (LLME), a lysosomotropic agent that kills actively phagocytic cells such as microglia[36]. Treatment of spinal cultures with 5-mM LLME killed approximately 60–70% of Mac2-positive cells; control cultures showed only mild neurotoxicity (**Fig. 8d**). Pretreatment of the cell cultures with LLME did not rescue motor neurons from the toxicity of recombinant SOD1. Although these results indicate that extracellular SOD1 mutant can injure motor neurons independently of microglial activation, the role of microgliosis in motor neuron death cannot be excluded. The viability of motor neurons was affected by extracellular CgA or LPS after longer time exposures (**Fig. 8e**).

DISCUSSION

From the data presented here, we propose a novel pathogenic mechanism for ALS based on chromogranin-mediated secretion of misfolded SOD1 mutants (**Supplementary Fig. 6** online). This model is supported by the following findings: (i) chromogranins interact with ALS-linked SOD1 mutants but not with wild-type SOD1, (ii) chromogranins can promote selective secretion of mutant SOD1, (iii) mutant SOD1 is distributed in the TGN, (iv) extracellular mutant SOD1 can

trigger microgliosis and neuronal death and (v) CgA expression is induced in reactive astrocytes.

It is unclear how the mutant SOD1 proteins are being recruited in the ER-Golgi secretory granule pathway to interact with chromogranins. SOD1 protein has no signal sequence. It is possible that an increased hydrophobicity of mutant SOD1 underlies its translocation in the ER-Golgi pathway, as reported for fibroblast growth factor-16 (ref. 37). The cytosolic soluble protein SOD1 normally maintains its hydrophilicity through intramolecular disulfide bonds. However, mutant SOD1 proteins are readily monomerized by a reducing environment[38], resulting in exposure of hydrophobic regions that can be recognized by Hsp proteins[16]. Once recruited into the ER-Golgi system, it is plausible that oxidative conditions might promote the formation of oligomers, as detected in **Figure 3a**. Our findings are consistent with a previous report that mutant SOD1, but not wild-type SOD1, can induce ER stress when transfected into COS-7 cells, with accumulation of mutant SOD1 in or on the ER[39]. Although we cannot exclude the possibility of a gain of toxic function due to ER stress, our data demonstrate that secretion of mutant SOD1 may represent a toxic pathway which would be in line with the non-cell-autonomous nature of ALS[14].

It is still unclear how mutant SOD1 associates with chromogranins in the ER-Golgi network. The results from our yeast two-hybrid interaction studies support a direct association. Moreover, *in vitro* binding of recombinant CgA with mutant SOD1, but not with wild-type SOD1, was also confirmed (data not shown). The presence of Hsp70-like motifs in both CgB and CgA may explain why chromogranins interact with mutant forms of SOD1, but not with wild-type SOD1. Mutant SOD1 proteins are known to show altered solubility and interact with heat shock/stress proteins[15,16].

Previous studies have shown that wild-type SOD1 can be secreted from cultured astrocytes[40] or thymus-derived cells[41]. Moreover, it has been reported that both wild-type and mutant SOD1 species are detected in the cerebrospinal fluid of both transgenic rats[34] carrying human SOD1 and ALS patients with the SOD1 mutation[35]. Our data together with these observations support the idea that both wild-type and mutant SOD1 proteins may be secreted through non-classical secretory pathways[42]. In addition, we propose a chaperone-like function for chromogranins in mediating the selective secretion of misfolded SOD1 mutants through the ER-Golgi network. In a recent study[35] with NSC34 cells, the secretion was interpreted as being beneficial because the extrusion of mutant SOD1 attenuated formation of toxic intracellular inclusions, ameliorating cell survival. That study did not, however, consider the presence of glial cells in motor neuron environment *in vivo* or the possibility that the disease in not strictly cell autonomous[14]. Conversely, we posit that secretion of mutant SOD1 mediated by chromogranins is deleterious because extracellular mutant SOD1 proteins caused microgliosis and death of embryonic motor neurons in mixed cultures (**Fig. 8**). Unlike secreted mutant SOD1, extracellular wild-type SOD1 probably has protective properties. Our data suggest that extracellular wild-type SOD1 suppresses extracellular inflammation, perhaps through an antioxidant effect (**Fig. 7c**), which would be consistent with the finding that intraspinal infusion of exogenous wild-type SOD1 in G93A SOD1 transgenic rats prolonged their lifespan[34].

From our *in situ* hybridization data and immunohistochemistry of spinal cord samples, it seems that chromogranin expression is elevated in both motor neurons and interneurons (**Supplementary Fig. 2**). Therefore, as depicted in our proposed pathogenic scheme (**Supplementary Fig. 6**), we view interneurons as important contributors to the secretion of chromogranins and mutant SOD1 complexes in the vicinity of motor neurons. In this model, it is the burden of extracellular mutant SOD1 in close proximity to motor neurons that would increase the risk of damage. Even though interneurons and motor neurons themselves would be the predominant source of extracellular mutant SOD1 mediated by chromogranin interactions, mutant SOD1 secreted by other pathways from other cells such as microglia and astrocytes could also contribute to pathogenesis. Though the deleterious effects of intracellular mutant SOD1 can not be excluded, our model of toxicity based on secreted mutant SOD1 is compatible with the idea that the disease is not autonomous to motor neurons[14].

Although the exact mechanisms underlying the microgliosis and neurotoxicity of extracellular mutant SOD1 remain to be elucidated, various deleterious effects of misfolded SOD1 proteins may occur through generation of hydroxyl radicals[7], toxic oligomers[11] or amyloid-like filaments[43]. This model would support a linkage between inflammation and ALS pathogenesis[44,45]. Many factors may contribute to motor neuron death in the context of inflammation. Proinflammatory molecules such as TNF-α, Fas ligand or nitric oxide may act as mediators of motor neuron death[8]. Microglial activation alone is not usually sufficient to induce motor neuron death. For instance, induction of innate immunity by intraperitoneal injection of LPS does not injure motor neurons[44]. Chronic LPS administration precipitated ALS in mice, however, supporting the view that chronic inflammation may constitute a risk factor[44]. Yet, our data demonstrate that elimination of microglia by LLME did not alter survival of motor neurons and that LPS is much less toxic to motor neurons than mutant SOD1 in mixed embryonic spinal cord cultures (**Fig. 8b,e**). It is noteworthy that mutant SOD1, and to some extent wild-type SOD1, can be converted to toxic species even in absence of copper and zinc (**Fig. 8c**). This concurs with previous reports about the misfolded nature of apo-state SOD1 (refs. 16,43).

In conclusion, our results suggest a novel function for chromogranins in mediating the secretion of misfolded SOD1 mutants, a potentially toxic pathway that can induce inflammation and neuronal death. In future studies, it will be of interest to determine whether chromogranin-mediated secretion may be applicable to other neurodegenerative diseases that involve misfolded proteins.

METHODS

Materials. Commercially available antibodies are listed in **Supplementary Methods** online. The Golgi marker plasmid DsRed-Golgi, which carries the Golgi-targeting sequence of the human gene encoding β1,4-galactosyl transferase, was a generous gift from Y. Imai (RIKEN Brain Science Institute).

To generate an antibody specific to the N′ terminus of mouse CgA, we immunized rabbits with the peptide CLPVNSPMTKGDTKVMK, which encodes the amino terminal residues of mature mouse CgA (amino acids 18–35). The antisera were purified with an affinity column coupled with the same antigen. The titer and specificity were investigated by western blotting (**Supplementary Fig. 4**).

The recombinant proteins of human SOD1 (wild-type and mutant) and mouse CgA were generated from *Escherichia coli* as described in **Supplementary Methods**.

Transgenic mice. Transgenic mice harboring the G93A mutant of human *SOD1* (*B6SJL-TgN[SOD1-G93A]^{dl}1Gur*, *B6SJL-TgN[SOD1-G93A]1Gur*) and those harboring wild-type human *SOD1* (*C57Bl/6-TgN[SOD1]3Cje*, *hSOD1^{WT}*) were purchased from The Jackson Laboratory. Transgenic mice carrying G37R *SOD1* (line 29) were a kind gift from D. Cleveland (University of California, San Diego) and were housed and bred with C57Bl/6 mice. We selected these mouse lines because they were readily available to us. Since we maintain a larger colony of G37R *SOD1* (line 29) mice, most of our experiments involving mouse analysis were done with this line. Mice were treated with 10% chloral hydrate for anesthesia before they were perfused or killed. Animals were handled in accordance with the approved protocol by the animal experiment committees at RIKEN Brain Science Institute and by the Comité de Protection des Animaux de l'Université Laval.

Yeast two-hybrid screening. The plasmid *pGilda* carrying the G93A *SOD1* mutant was generated as bait for library screening. Yeast two-hybrid analysis (LexA/transactivation system) was performed on a cDNA library (1.5 10^6 independent clones) ligated into the *pJG4,5* plasmid from the total spinal cords of five preclinical transgenic mice carrying human G93A *SOD1* (*B6SJL-Tg(SOD1-G93A)1Gur/J*). Yeast two-hybrid screening was carried out using the Matchmaker Two-Hybrid System (Clontech) according to the manufacturer's protocol. There were 250 blue colonies that survived on the agar plates that contained galactose/raffinose and X-gal, but lacked tryptophan, histidine, leucine and uracil. All 250 were sequenced.

Plasmids, cell culture and transfection. Expression plasmids harboring human *SOD1* (wild-type, A4V, G85R or G93A) were prepared as reported previously[11]. The full-length murine genes encoding CgA (*Chga*) or CgB (*Chgb*) were cloned by RT-PCR using polyA-RNA from total brain of adult normal mice of the C57Bl/6 strain. See **Supplementary Methods** and **Supplementary Table 1** online for construction of EGFP-tagged CgB or deletion mutants of CgB. Cells from the murine neuroblastoma cell line Neuro2a, from the mouse fibroblast cell line NIH3T3 and COS-7 monkey ovary cells were maintained in nutrient medium containing 10% fetal bovine serum in the Dulbecco's minimal essential medium (DMEM, Sigma). The mouse microglial BV2 cells were cultured in DMEM-F12 Ham's (DF) medium containing 10% FBS. Cells were used for transfection using Lipofectamine Plus (Invitrogen) according to the manufacturer's protocol.

Immunoblotting and immunoprecipitation of cultured cells. Cells were lysed in TNT-G buffer consisting of 50 mM Tris-HCl (pH 7.4), 150 mM NaCl and 1% Triton-X100 with protease inhibitor cocktail (Roche) 24 h after the transfection. The cell lysates were incubated with anti-FLAG M2 agarose affinity gel (Sigma) for 1 h at 4 °C and were eluted with 4% SDS sample buffer. Samples were resolved by SDS-PAGE and transferred to a PVDF membrane (Polyscreen, PerkinElmer). A western blot image was obtained using a chemiluminescence detection kit (PerkinElmer).

Immunofluorescence and immunohistochemistry. Fixation of the cells and preparation of spinal cord slices is described in **Supplementary Methods.** After blocking, cultures or sections were incubated with primary antibodies and subsequently with corresponding fluorescent secondary antibodies (Alexa, Invitrogen) or with biotinylated secondary antibodies visualized by the avidin-biotin-immunoperoxidase complex (ABC) method using a Vectastain ABC kit (Vector Laboratories) and 3.3′-diaminobenzidine tetrahydrochloride (DAB; Sigma). The dilution rate of the primary antibodies is indicated in **Supplementary Methods.** Cells and tissue sections were observed by confocal laser microscopy (Olympus).

Subcellular fractionation of the spinal cord lysates. Spinal cord tissues from different ages of human *SOD1* transgenic mice were subcellularly fractionated into cytosolic, heavy and light membrane fractions, as described in **Supplementary Methods.** The protein concentration was determined by Bradford assay (BioRad), and an equal amount of protein was analyzed by western blotting. The percentage distribution of hSOD1 in post-nuclear fractions was also obtained by densitometric analysis and calculation of proportion from initial volume.

Sucrose-gradient ultracentrifugation of microsome fraction from spinal cord lysates. The light membrane (microsomal) fraction from spinal cord of *G37R SOD1* mice was further separated by sucrose gradient ultracentrifugation as previously described[46], with minor modifications that are decribed in **Supplementary Methods.** After overnight ultracentrifugation in sucrose cushions (5%, 30% and 40%), one-tenth (0.42 ml) was taken from the top of each sample, and the pellet was resuspended in MBS with 2 mM EDTA and 1% Triton-X100, and then concentrated using a centrifugal filter (Millipore) to 100 µl. Each fraction (20 µl) was separated by SDS-PAGE and analyzed by western blotting.

Immuno-isolation of TGN. To obtain pure preparations of TGN, we generated rabbit polyclonal antibody specific to the amino terminal peptides (CEGKRSKVTRRPKASDYQRLNLKL) of mouse/rat TGN38, a surface marker of TGN[47]. This anti-TGN38 or rabbit control IgG was bound to protein G-coated magnetic beads (Dynal) and was incubated with precleared post-mitochondrial fractions (described in more detail in **Supplementary Methods**). After washing, immunoprecipitates were eluted by 4% SDS sampling buffer and analyzed by western blotting with human SOD1-specific antibody (StressGen).

Immunoprecipitation of spinal cord lysates. The post-mitochondrial fractions of spinal cords were prepared by the same protocol as those in the immuno-isolation experiments. Rabbit polyclonal antibodies to CgA or CgB (Santa Cruz) or rabbit control IgG was bound to protein G-coated magnetic beads and incubated with precleared lysates, as described in **Supplementary Methods.** Immunoprecipitates were analyzed by Western blotting with human SOD1-specific antibody (StressGen).

Immunoelectron microscopy. We used post-embedding immunohistochemistry for electron microscopic observation, in which ultra-thin sections on the nickel grids were processed for immunohistochemistry without osmication. Fixation of the mice and preparation of ultrathin sections are described in **Supplementary Methods.** After blocking, grids were incubated with primary antibodies in the same buffer at 4 °C overnight, followed by a reaction with immunogold-conjugated secondary antibody (10 nm or 5 nm) for 1 h at 22 °C. For double staining, grids were further processed using another immunoreaction with a different primary and the secondary antibody with differently sized gold particles. Grids were observed by a TECNAI 12 electron microscope (FEI company).

Secretion assays. COS-7 and NIH3T3 cells were used in secretion experiments as non-neuronal cells lacking secretory granules[33]. At 24 h after transfection, cells plated onto a 6-well culture dish were washed in prewarmed PBS twice. Cells were incubated in basal secretion medium containing 10 mM HEPES, 129 mM NaCl, 5 mM $NaHCO_3$, 4.8 mM KCl, 1.2 mM $MgCl_2$, 1.2 mM KH_2PO_4, 1 mM $CaCl_2$ and 2.8 mM glucose (pH 7.4) for 1 h, and then treated with 1 ml of secretagogue-containing medium (stimulation buffer: 10 mM Hepes, 79 mM NaCl, 5 mM $NaHCO_3$, 50 mM KCl, 1.2 mM KH_2PO_4, 1.2 mM $MgCl_2$, 2 mM $BaCl_2$, 2.8 mM glucose, pH 7.4) for 15 min. In some experiments, Brefeldin A (BFA, 5 µM) was applied before exposure to stimulation medium. Lactacystin was applied in some assays 3 h after transfection and before incubation with basal buffer. We then collected 950 µl of medium and centrifuged it for 5 min at 1,000*g* to remove the debris. The supernatants were concentrated by a protein concentrator with 3.5 kDa cut-off (Millipore) to 60 µl, followed by western analysis. Secreted SOD1 was estimated by standardization with intracellular SOD1 in total cell lysates.

Primary cultures from embryonic spinal cord of transgenic mice carrying human *SOD1* (wild-type or *G37R*) were also investigated by secretion analysis. Cultures were prepared as explained below. Cell suspension from one spinal cord was plated onto one chamber in a six-well culture plate coated with polyethyleneimine. Secretion experiments were done after 14 d of culture *in vitro* using the protocol described above.

The content of LDH in the culture medium was measured in the medium 24 h after transfection using an LDH assay kit (Promega) according to the manufacture's protocol. Cells transfected with empty vector were used as a control.

Semi-quantitative reverse transcription PCR of microglial cell lines. Neuro2a cells were co-transfected with *pcDNA-SOD1* (wild-type, *G85R* or *G93A*) and *pcDNA3-CgA* in DF medium containing 10% FBS. At 16 h after transfection, the conditioned medium was transferred into the culture wells where BV2 cells had been previously plated, then further incubated for 24 h. Alternatively, BV2 cells were treated directly with recombinant proteins for 24 h. Then, cells were washed twice in PBS and total RNA was extracted using Trizol (Invitrogen). RT-PCR was conducted using oligo-dT primers according to the manufacturer's protocol (Invitrogen). The sequence of primer pairs is shown in **Supplementary Table 2** online. The gel images of PCR products obtained from illuminator were scanned, and densitometric analysis was performed using Scion image (Scion Corp.).

Primary culture of mouse embryonic spinal cord. Dissociated cultures of embryonic murine spinal cord were grown as previously described[11]. The spinal

cultures were treated at 11 or 14 d after plating. Motor neurons were identified as large cells labeled with SMI32 and active microglia were detected with Mac2-specific antibody. Confocal microscopy images were obtained from eight randomly selected fields, and immunoreactive cells were counted by computer. In several experiments, microglia were eliminated by a 16-h treatment with LLME[36] before exposure to recombinant SOD1 proteins. In preliminary experiments, we noticed that 5-mM LLME for 16 h killed approximately 60–70% of Mac2-positive cells. The number of cells was calculated as cells per mm^2 and averaged. Statistical significance was evaluated by single-factor ANOVA (analysis of variance) following Scheffe's method.

Note: Supplementary information is available on the Nature Neuroscience website.

ACKNOWLEDGMENTS

We thank R. Janvier for sample preparation for immunoelectron microscopy and B. Gentil for advice on experimental procedures. The technical help from G. Soucy, S.A. Ezzi (Laval University) and J. Kurisu (RIKEN Brain Science Institute) is appreciated. We thank D. Cleveland (University of California San Diego) for the G37R *SOD1* transgenic mice and Y. Imai for the *DsRed-Golgi* plasmid. This work was supported by the Canadian Institutes of Health Research (CIHR), the Robert Packard Centre for ALS Research at Johns Hopkins, the ALS Association (USA), the ALS Society of Canada, the Japan Society for the Promotion of Science (JSPS) and the Japan Foundation for Neuroscience and Mental Health. J.-P.J. holds a Canada Research Chair in Neurodegeneration. M.U. is a recipient of a Uehara Memorial Foundation research fellowship and a postdoctoral fellowship from CIHR.

COMPETING INTERESTS STATEMENT

The authors declare that they have no competing financial interests.

Published online at http://www.nature.com/natureneuroscience/
Reprints and permissions information is available online at http://npg.nature.com/reprintsandpermissions/

1. Rosen, D.R. *et al.* Mutations in Cu/Zn superoxide dismutase gene are associated with familial amyotrophic lateral sclerosis. *Nature* **362**, 59–62 (1993).
2. Gurney, M.E. *et al.* Motor neuron degeneration in mice that express a human Cu,Zn superoxide dismutase mutation. *Science* **264**, 1772–1775 (1994).
3. Subramaniam, J.R. *et al.* Mutant SOD1 causes motor neuron disease independent of copper chaperone-mediated copper loading. *Nat. Neurosci.* **5**, 301–307 (2002).
4. Wang, J., Xu, G. & Borchelt, D.R. High molecular weight complexes of mutant superoxide dismutase 1: age-dependent and tissue-specific accumulation. *Neurobiol. Dis.* **9**, 139–148 (2002).
5. Julien, J.P. Amyotrophic lateral sclerosis. unfolding the toxicity of the misfolded. *Cell* **104**, 581–591 (2001).
6. Cleveland, D.W. & Rothstein, J.D. From Charcot to Lou Gehrig: deciphering selective motor neuron death in ALS. *Nat. Rev. Neurosci.* **2**, 806–819 (2001).
7. Wiedau-Pazos, M. *et al.* Altered reactivity of superoxide dismutase in familial amyotrophic lateral sclerosis. *Science* **271**, 515–518 (1996).
8. Raoul, C. *et al.* Motoneuron death triggered by a specific pathway downstream of Fas: potentiation by ALS-linked SOD1 mutations. *Neuron* **35**, 1067–1083 (2002).
9. Durham, H.D., Roy, J., Dong, L. & Figlewicz, D.A. Aggregation of mutant Cu/Zn superoxide dismutase proteins in a culture model of ALS. *J. Neuropathol. Exp. Neurol.* **56**, 523–530 (1997).
10. Johnston, J.A., Dalton, M.J., Gurney, M.E. & Kopito, R.R. Formation of high molecular weight complexes of mutant Cu, Zn-superoxide dismutase in a mouse model for familial amyotrophic lateral sclerosis. *Proc. Natl. Acad. Sci. USA* **97**, 12571–12576 (2000).
11. Urushitani, M., Kurisu, J., Tsukita, K. & Takahashi, R. Proteasomal inhibition by misfolded mutant superoxide dismutase 1 induces selective motor neuron death in familial amyotrophic lateral sclerosis. *J. Neurochem.* **83**, 1030–1042 (2002).
12. Pramatarova, A., Laganière, J., Roussel, J., Brisebois, K. & Rouleau, G.A. Neuron-specific expression of mutant superoxide dismutase 1 in transgenic mice does not lead to motor impairment. *J. Neurosci.* **21**, 3369–3374 (2001).
13. Lino, M.M., Schneider, C. & Caroni, P. Accumulation of SOD1 mutants in postnatal motoneurons does not cause motoneuron pathology or motoneuron disease. *J. Neurosci.* **22**, 4825–4832 (2002).
14. Clement, A.M. *et al.* Wild-type nonneuronal cells extend survival of SOD1 mutant motor neurons in ALS mice. *Science* **302**, 113–117 (2003).
15. Shinder, G.A., Lacourse, M.C., Minotti, S. & Durham, H.D. Mutant Cu/Zn-superoxide dismutase proteins have altered solubility and interact with heat shock/stress proteins in models of amyotrophic lateral sclerosis. *J. Biol. Chem.* **276**, 12791–12796 (2001).
16. Urushitani, M. *et al.* CHIP promotes proteasomal degradation of familial ALS-linked mutant SOD1 by ubiquitinating Hsp/Hsc70. *J. Neurochem.* **90**, 231–244 (2004).
17. Taupenot, L., Harper, K.L. & O'Connor, D.T. The chromogranin-secretogranin family. *N. Engl. J. Med.* **348**, 1134–1149 (2003).
18. Rudolf, R., Salm, T., Rustom, A. & Gerdes, H.H. Dynamics of immature secretory granules: role of cytoskeletal elements during transport, cortical restriction, and f-actin-dependent tethering. *Mol. Biol. Cell* **12**, 1353–1365 (2001).
19. Li, J.Y., Leitner, B., Lovisetti-Scamihorn, P., Winkler, H. & Dahlström, A. Proteolytic processing, axonal transport and differential distribution of chromogranins A and B, and secretogranin II (secretoneurin) in rat sciatic nerve and spinal cord. *Eur. J. Neurosci.* **11**, 528–544 (1999).
20. Booj, S., Goldstein, M., Fischer-Colbrie, R. & Dahlstrom, A. Calcitonin gene-related peptide and chromogranin A: presence and intra-axonal transport in lumbar motor neurons in the rat, a comparison with synaptic vesicle antigens in immunohistochemical studies. *Neuroscience* **30**, 479–501 (1989).
21. Marksteiner, J. *et al.* Distribution of chromogranin B-like immunoreactivity in the human hippocampus and its changes in Alzheimer's disease. *Acta Neuropathol. (Berl.)* **100**, 205–212 (2000).
22. Rangon, C.M. *et al.* Different chromogranin immunoreactivity between prion and a-beta amyloid plaque. *Neuroreport* **14**, 755–758 (2003).
23. Schiffer, D., Cordera, S., Giordana, M.T., Attanasio, A. & Pezzulo, T. Synaptic vesicle proteins, synaptophysin and chromogranin A in amyotrophic lateral sclerosis. *J. Neurol. Sci.* **129** Suppl, 68–74 (1995).
24. Taupenot, L. *et al.* Chromogranin A triggers a phenotypic transformation and the generation of nitric oxide in brain microglial cells. *Neuroscience* **72**, 377–389 (1996).
25. Ciesielski-Treska, J. *et al.* Mechanisms underlying neuronal death induced by chromogranin A-activated microglia. *J. Biol. Chem.* **276**, 13113–13120 (2001).
26. Taylor, D.L., Diemel, L.T. & Pocock, J.M. Activation of microglial group III metabotropic glutamate receptors protects neurons against microglial neurotoxicity. *J. Neurosci.* **23**, 2150–2160 (2003).
27. Chanat, E., Weiss, U., Huttner, W.B. & Tooze, S.A. Reduction of the disulfide bond of chromogranin B (secretogranin I) in the trans-Golgi network causes its missorting to the constitutive secretory pathways. *EMBO J.* **12**, 2159–2168 (1993).
28. Cowley, D.J., Moore, Y.R., Darling, D.S., Joyce, P.B. & Gorr, S.U. N- and C-terminal domains direct cell type-specific sorting of chromogranin A to secretory granules. *J. Biol. Chem.* **275**, 7743–7748 (2000).
29. Li, J.Y., Kling-Petersen, A. & Dahlstrom, A. Influence of spinal cord transection on the presence and axonal transport of CGRP-, chromogranin A-, VIP-, synapsin I-, and synaptophysin-like immunoreactivities in rat motor nerve. *J. Neurobiol.* **23**, 1094–1110 (1992).
30. Kato, A. *et al.* Co-distribution patterns of chromogranin B-like immunoreactivity with chromogranin A and secretoneurin within the human brainstem. *Brain Res.* **852**, 444–452 (2000).
31. Stieber, A. *et al.* Disruption of the structure of the Golgi apparatus and the function of the secretory pathway by mutants G93A and G85R of Cu, Zn superoxide dismutase (SOD1) of familial amyotrophic lateral sclerosis. *J. Neurol. Sci.* **219**, 45–53 (2004).
32. Ciesielski-Treska, J. *et al.* Chromogranin A induces a neurotoxic phenotype in brain microglial cells. *J. Biol. Chem.* **273**, 14339–14346 (1998).
33. Huh, Y.H., Jeon, S.H. & Yoo, S.H. Chromogranin B-induced secretory granule biogenesis: comparison with the similar role of chromogranin A. *J. Biol. Chem.* **278**, 40581–40589 (2003).
34. Turner, B.J. *et al.* Impaired extracellular secretion of mutant superoxide dismutase 1 associates with neurotoxicity in familial amyotrophic lateral sclerosis. *J. Neurosci.* **25**, 108–117 (2005).
35. Jacobsson, J., Jonsson, P.A., Andersen, P.M., Forsgren, L. & Marklund, S.L. Superoxide dismutase in CSF from amyotrophic lateral sclerosis patients with and without CuZn-superoxide dismutase mutations. *Brain* **124**, 1461–1466 (2001).
36. Sharpless, N. *et al.* The restricted nature of HIV-1 tropism for cultured neural cells. *Virology* **191**, 813–825 (1992).
37. Miyakawa, K. & Imamura, T. Secretion of FGF-16 requires an uncleaved bipartite signal sequence. *J. Biol. Chem.* **278**, 35718–35724 (2003).
38. Tiwari, A. & Hayward, L.J. Familial amyotrophic lateral sclerosis mutants of copper/zinc superoxide dismutase are susceptible to disulfide reduction. *J. Biol. Chem.* **278**, 5984–5992 (2003).
39. Tobisawa, S. *et al.* Mutant SOD1 linked to familial amyotrophic lateral sclerosis, but not wild-type SOD1, induces ER stress in COS7 cells and transgenic mice. *Biochem. Biophys. Res. Commun.* **303**, 496–503 (2003).
40. Lafon-Cazal, M. *et al.* Proteomic analysis of astrocytic secretion in the mouse. Comparison with the cerebrospinal fluid proteome. *J. Biol. Chem.* **278**, 24438–24448 (2003).
41. Cimini, V. *et al.* CuZn-superoxide dismutase in human thymus: immunocytochemical localisation and secretion in thymus-derived epithelial and fibroblast cell lines. *Histochem. Cell Biol.* **118**, 163–169 (2002).
42. Nickel, W. The mystery of nonclassical protein secretion. A current view on cargo proteins and potential export routes. *Eur. J. Biochem.* **270**, 2109–2119 (2003).
43. Elam, J.S. *et al.* Amyloid-like filaments and water-filled nanotubes formed by SOD1 mutant proteins linked to familial ALS. *Nat. Struct. Biol.* **10**, 461–467 (2003).
44. Nguyen, M.D., D'Aigle, T., Gowing, G., Julien, J.P. & Rivest, S. Exacerbation of motor neuron disease by chronic stimulation of innate immunity in a mouse model of amyotrophic lateral sclerosis. *J. Neurosci.* **24**, 1340–1349 (2004).
45. Zhu, S. *et al.* Minocycline inhibits cytochrome c release and delays progression of amyotrophic lateral sclerosis in mice. *Nature* **417**, 74–78 (2002).
46. Parkin, E.T., Hussain, I., Karran, E.H., Turner, A.J. & Hooper, N.M. Characterization of detergent-insoluble complexes containing the familial Alzheimer's disease-associated presenilins. *J. Neurochem.* **72**, 1534–1543 (1999).
47. Stephens, D.J. & Banting, G. Direct interaction of the trans-Golgi network membrane protein, TGN38, with the F-actin binding protein, neurabin. *J. Biol. Chem.* **274**, 30080–30086 (1999).

The neuropeptide head activator is a high-affinity ligand for the orphan G-protein-coupled receptor GPR37

Meriem Rezgaoui[1], Ute Süsens[1], Atanas Ignatov[1], Mathias Gelderblom[2], Günter Glassmeier[3], Inga Franke[1], Jens Urny[1], Yuzuru Imai[4], Ryosuke Takahashi[4] and H. Chica Schaller[1,*]

[1]Zentrum für Molekulare Neurobiologie Hamburg, [2]Klinik und Poliklinik für Neurologie, and [3]Institut für Angewandte Physiologie, Universitätsklinikum Hamburg-Eppendorf, Martinistr. 52, 20246 Hamburg, Germany
[4]RIKEN Brain Science Institute, Saitama 351-0198, Japan
*Author for correspondence (e-mail: schaller@zmnh.uni-hamburg.de)

Accepted 26 October 2005
Journal of Cell Science 119, 542-549 Published by The Company of Biologists 2006
doi:10.1242/jcs.02766

Summary

The neuropeptide head activator (HA) is a mitogen for mammalian cell lines of neuronal or neuroendocrine origin. HA signalling is mediated by a G-protein-coupled receptor (GPCR). Orphan GPCRs with homology to peptide receptors were screened for HA interaction. Electrophysiological recordings in frog oocytes and in mammalian cell lines as well as Ca^{2+} mobilisation assays revealed nanomolar affinities of HA to GPR37. HA signal transduction through GPR37 was mediated by an inhibitory G protein and required Ca^{2+} influx through a channel of the transient receptor potential (TRP) family. It also required activation of Ca^{2+}-dependent calmodulin kinase and phosphoinositide 3-kinase. Respective inhibitors blocked HA signalling and HA-induced mitosis in GPR37-expressing cells. HA treatment resulted in internalisation of GPR37. Overexpression of GPR37 led to aggregate formation, retention of the receptor in the cytoplasm and low survival rates of transfected cells, confirming the notion that misfolded GPR37 contributes to cell death, as observed in Parkinson's disease.

Key words: G-protein-coupled receptor, GPR37, Head activator, Pael receptor, Parkinson, Signal transduction

Introduction

The undecapeptide head activator (HA) was originally isolated and characterised from hydra, where it mediates head-specific growth and differentiation processes, hence its name. In hydra, HA is produced by nerve cells and is stored in neurosecretory granules, from which it is released to initiate head regeneration and budding, and to maintain the normal head-to-foot morphology of hydra. At the cellular level, HA promotes proliferation of all cell types of hydra by acting as mitogen in the G2-mitosis transition; as for early mammalian development, this transition is the most important checkpoint to control cell-cycle progression. At higher concentrations, HA acts on the determination of stem cells to head-specific fates (Schaller et al., 1996).

HA was isolated with identical sequence from mammalian brain and intestine (Bodenmuller and Schaller, 1981). In adult mammals, HA enhances neurite outgrowth and is neuroprotective. HA is present during early mammalian development and is expressed in cells of the nervous and neuroendocrine system. Like in hydra, HA stimulates entry into mitosis and proliferation of cell lines derived from such origins. The signalling cascade from HA to mitosis includes activation of an inhibitory G protein and requires Ca^{2+} influx, downregulation of adenylyl cyclase and hyperpolarisation of the membrane potential (Kayser et al., 1998; Niemann and Schaller, 1996; Ulrich et al., 1996). For Ca^{2+} influx, a transient receptor potential (TRP)-like channel is responsible, which can be regulated by growth factors, such as insulin growth factor I (IGF-I) and platelet-derived growth factor (PDGF) (Kanzaki et al., 1999), and by HA (Boels et al., 2001). The increase in intracellular Ca^{2+} then triggers influx of K^+ through a Ca^{2+}-activated K^+ channel, leading to hyperpolarisation, which is an absolute requirement for entry into mitosis (Kayser et al., 1998).

In the search for receptors mediating the action of HA on stimulating mitosis in mammalian cells, we concentrated on orphan G-protein-coupled receptors (GPCRs) reacting with small peptides as ligands. GPCRs are the largest family of cell-surface receptors that mediate transduction of signals from the extracellular environment to intracellular effectors. They contain seven transmembrane domains and are activated by ligands of extremely different molecular origins and sizes including light, ions, metabolic intermediates, amino acids, nucleotides, lipids, peptides and proteins. These ligands primarily interact with the extracellular domains, but in part also with transmembrane regions of GPCRs. The classification of GPCRs into subfamilies is primarily based on their homology within the heptahelical structure (Frederiksson et al., 2003), but also on extracellular domains, and has been used to predict ligands for orphan receptors (Boels and Schaller, 2003; Ignatov et al., 2003a; Ignatov et al., 2003b). To find a receptor for HA, we concentrated on GPCR subfamilies reacting with small peptides as ligands.

Several orphan receptors failed to show interactions with HA, including GPR6 and GPR12, for which we found lysophospholipids as cognate ligands (Ignatov et al., 2003a;

Ignatov et al., 2003b). HA had no effect on GPR99, GPR100, GalRL, GPR1, GPR7, GPR8, GPR19, GPR75 and SALPR, just to name a few. Of special interest was a sub-branch of GPCRs that regulate cellular proliferation, namely the endothelin, bombesin and neuromedin receptors. Two orphan receptors are part of this group: GPR37 and GPR37L1 (Marazziti et al., 2001). We focused our interest on GPR37 because of its prominent expression in neurons of the brain compared with a more glial location of GPR37L1 (Marazziti et al., 1997; Zeng et al., 1997). GPR37 has also been isolated and characterised as a substrate for the ubiquitin ligase parkin, hence its alternative name – parkin-associated endothelin-like receptor (Pael R) (Imai et al., 2001). GPR37 was shown to fold improperly in the absence of parkin, and its aggregation to insoluble complexes results in endoplasmic reticulum stress (Imai et al., 2001; Imai et al., 2003). This leads to preferential loss of dopaminergic neurons in the substantia nigra and contributes to neurodegeneration in Parkinson's disease (Yang et al., 2003). Accumulation of GPR37 in Lewy bodies in the brain of patients with Parkinson's disease supports this notion (Murakami et al., 2004).

To study a possible interaction of HA with GPR37, various assay systems were used that allow detection, directly or indirectly, of ligand-receptor interactions. In this paper, we present evidence that HA is a high-affinity ligand for GPR37.

Results

HA stimulates internalisation of GPR37 in COS-7 cells

We tried to express GPR37 heterologously in Chinese hamster ovary (CHO-K1) cells, in human embryonic kidney (HEK-293) cells and in green monkey kidney (COS-7) cells. Transient transfection efficiencies in HEK-293 and CHO-K1 cells were far below 5%, and cells expressing GPR37 looked sick and decreased in number at 48 hours compared with 24 hours after transfection. Transfection efficiencies in COS-7 cells were better and reached levels in the range of 15-30% (Fig. 1A). COS-7 cells were therefore suitable for experiments with individual, transfected cells. There was no difference in expression levels between GPR37 with (Fig. 1B) and without (Fig. 1C) FLAG tag at the C-terminus. This indicated that the tag did not interfere with GPR37 protein biosynthesis and localisation. GPR37 immunoreactivity was visible in the cytoplasm of transfected COS-7 cells, but also extended to cell protrusions, hinting at cell-surface expression (Fig. 1B,C). Cell-surface expression was confirmed by treating living cells before fixation with a monoclonal antibody against GPR37 (Fig. 1D) that reacts with extracellular epitopes of GPR37 (Imai et al., 2001).

HA treatment of COS-7 cells transiently transfected with GPR37-FLAG led to internalisation of the receptor. This was visible as disappearance of the GPR37-FLAG immunoreactivity from the protrusions after 10 minutes (compare Fig. 1E and F), and as translocation into the cytoplasm after 20 minutes (Fig. 1G). Protrusions started to show FLAG staining again after 30-60 minutes (Fig. 1H,I).

GPR37 aggregation is prevented by stable inducible expression in HEK-293 cells

Transient expression of GPR37 led in all cell lines assayed to aggregation of complexes with apparent molecular masses of 250 kDa (Fig. 2A). Surface biotinylation showed that only the monomeric receptor appeared at the outer cell membrane (Fig. 2B), indicating that most of the overproduced GPR37 was not properly folded, stayed in the cytoplasm and was probably

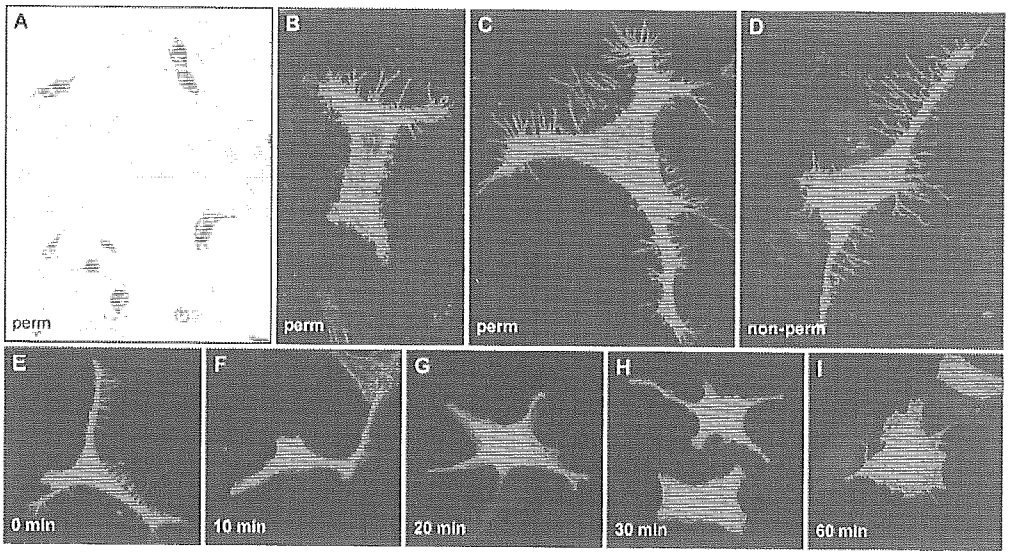

Fig. 1. GPR37 is expressed at the cell surface of COS-7 cells and internalises after HA treatment. (A-I) COS-7 cells were transfected with GPR37 with (B,D-I) or without (A,C) FLAG tag, immunostained with anti-GPR37 antibody (A,C,D) or with anti-FLAG antibody (B,E-I) and visualised with alkaline phosphatase-coupled secondary antibodies for light microscopy (A) or with Cy3-coupled antibodies for confocal analysis (B-I). Cells were permeabilised (perm) by fixation with 1% acetic acid in ethanol and by washing with Triton X-100, except in D, where living cells were incubated with the primary antibody before fixation (non-perm) to show surface staining. (E-I) COS-7 cells 48 hours after transfection with GPR37-FLAG were treated at 37°C with 2 nM HA for 0, 10, 20, 30 and 60 minutes, respectively, and immunostained with anti-FLAG antibody.

degraded (Imai et al., 2001). To prevent aggregation and subsequent degradation, we integrated GPR37 stably into HEK-T-REx cells with a construct that allowed induction by tetracycline (HEK-T-REx–GPR37). Incubation of cells with the tetracycline derivative doxycycline for 24 hours resulted in production predominantly of the monomeric form of GPR37 (Fig. 2C, first lane). Without doxycycline induction, GPR37 was not detectable (Fig. 2C, second lane). Confocal image analysis revealed that, after induction with doxycycline, GPR37 localised mainly to the outer cell membrane, both in permeabilised (Fig. 2D) and non-permeabilised cells (Fig. 2F). The non-induced cells showed no GPR37 immunoreactivity (Fig. 2E,G). To study internalisation, HEK-T-REx–GPR37 cells were incubated in defined medium for 24 hours with doxycycline to induce GPR37 expression. Subsequent treatment with HA for 10 minutes led to rapid internalisation of GPR37 (Fig. 2H,I). This internalisation was much faster in HEK than in COS-7 cells, probably as a result of differences in -arrestin levels (Ménard et al., 1997).

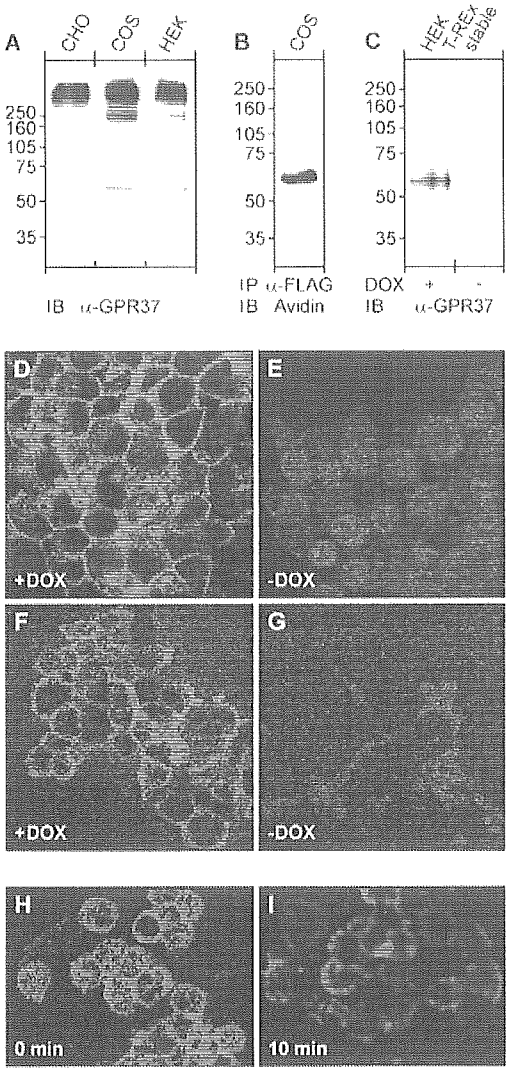

Fig. 2. Inducible, stable expression of GPR37 prevents aggregate formation. (A) CHO-K1, COS-7 and HEK-293 cells were transiently transfected with GPR37, and membrane fractions were assayed by immunoblotting (IB) with anti-GPR37 antibody (-GPR37). (B) COS-7 cells transiently transfected with GPR37-FLAG were cell-surface biotinylated, and the solubilised membrane fraction was immunoprecipated (IP) with anti-FLAG antibody (-FLAG) and visualised after immunoblotting with avidin. (C) GPR37 was introduced stably into the flip-in cell line HEK-T-REx, where GPR37 expression is inducible by doxycycline (DOX). Membrane fractions were subjected to western blotting with anti-GPR37 antibody (-GPR37) with (first lane) and without (second lane) induction for 24 hours with doxycycline. (D-I) HEK-T-REx–GPR37 cells with (D,F,H,I) and without (E,G) doxycycline induction for 24 hours were immunostained with anti-GPR37(R2) antibody after permeabilisation (D,E) and with anti-GPR37 antibody without permeabilisation (F-I). (H,I) HEK-T-REx–GPR37 cells were treated with 2 nM HA for 0 and 10 minutes at 37°C, respectively, fixed with 2% formaldehyde for 10 minutes and subsequently immunostained with anti-GPR37 antibody.

HA binds to GPR37

To show direct interaction of HA with GPR37, COS-7 cells were analysed after incubation with 2 nM HA by fluorescence resonance energy transfer (FRET). Localisation of HA was detected with a HA-specific polyclonal antiserum and was visualised with a Cy2-coupled secondary antibody (green). To detect GPR37, monoclonal antibodies directed against the extracellular domain of human GPR37 were used in combination with a Cy3-coupled secondary antibody (red). Fig. 3A-D shows a typical example of FRET between HA and ectodomains of GPR37. After bleaching a discrete area in a GPR37-positive cell (Fig. 3A,B), an increase in HA fluorescence was observed (Fig. 3C,D). The difference in staining pattern is due to the fact that COS-7 cells, in addition to GPR37, express endogenous HA receptor(s) (Boels et al., 2001). The experiment was repeated several times on different days yielding similar results. On average, the calculated energy-transfer efficiencies were in the range of 19.4±4.5%, indicating the close association of GPR37 and HA. Non-transfected cells were negative, and no transfer of signal was obtained if an antibody against the FLAG tag at the C-terminus of GPR37 was used (data not shown).

For visualisation of HA binding to GPR37, a fluorescent derivative of HA was produced. For this purpose, the fluorophore Cy3B was coupled to the -amino group of Lys7 of HA. The neuroblastoma cell line NH15-CA2, which reacts with HA (Ulrich et al., 1996) and endogenously expresses GPR37 (Fig. 3E), was used as positive control. Binding of Cy3B-labelled HA to NH15-CA2 cells was observed starting from a concentration of 50 nM, with optimal binding at 150 nM, achieved after incubation for 10 minutes at 37°C (Fig. 3F). Pre-incubation with unlabelled HA for 50 minutes prevented Cy3B-HA binding (Fig. 3G). Cy3B-labelled HA did not bind to HEK-T-REx–GPR37 cells without induction of GPR37 expression by doxycycline (Fig. 3H), but reacted after induction for 24 hours with doxycycline (Fig. 3I). Pre-incubation with unlabelled HA inhibited binding (Fig. 3J), demonstrating that the two ligands compete for the same receptor and that the receptor is either occupied or, more likely, internalised after interaction with HA.

HA induces an increase in Ca^{2+} mobilisation in cells expressing GPR37

To confirm the interaction of HA with GPR37, Ca^{2+} mobilisation was measured in CHO-K1 cells stably

transfected with apoaequorin as Ca^{2+} sensor and with the promiscuous G-protein subunit G 16 for signal enhancement. After reconstitution with the aequorin cofactor coelenterazine, agonist action was monitored as increase in bioluminescence (Stables et al., 1997). Since GPR37 was not sufficiently expressed in this cell line (CHO) by transient transfection, a stable cell line was established that, in addition to G 16 and apoaequorin, also expressed GPR37 (CHO-GPR37). Treatment of these cells with HA dose dependently led to an increase in Ca^{2+} mobilisation with an EC_{50} value of 3.3 nM (Fig. 4A). To our surprise, an endogenous response was also observed (Fig. 4A). Northern blots were negative, but immunocytochemistry (Fig. 4B) and western blots (Fig. 4C) probed with an antiserum against the very conserved intracellular C-tail confirmed presence of GPR37 in CHO cells. The hippocampal mouse cell line HT22, expressing GPR37 endogenously, was used as a positive control (Fig. 4C). The active monomeric form of GPR37 was predominantly present both in CHO-GPR37 and HT22 cells.

HA stimulates a current increase in frog oocytes expressing GPR37

In our hands, the frog oocyte system has proven to be very reliable and robust for studying the interaction of ligands with orphan GPCRs (Ignatov et al., 2003a; Ignatov et al., 2003b). Since HA signal transduction for mitotic stimulation is coupled to an inhibitory G protein (Kayser et al., 1998; Ulrich et al., 1996), frog oocytes were injected not only with complementary RNAs (cRNAs) coding for human GPR37, but also with cRNAs coding for the G-protein-coupled inwardly rectifying K^+ channel GIRK, which is activated by subunits of inhibitory G proteins (Kofuji et al., 1995). The concatemer between GIRK1 and GIRK2 (GIRK1/2) was chosen to enhance the current increase and improve the signal to noise ratio (Wischmeyer et al., 1997). Treatment with HA led to an additional increase in the basal inward current induced by changing the external bath medium to high K^+ in oocytes expressing GPR37 together with GIRK1/2 (Fig. 5A). A minute, negligible response was also obtained with medium alone (Fig. 5A). The effect of HA was concentration dependent, and a dose-response curve yielded an EC_{50} value of 5.6 nM (Fig. 5B). Since HA was diluted about twofold by addition to the oocyte bath medium, this EC_{50} value is in agreement with that obtained in the Ca^{2+}-mobilisation assay in CHO cells. Oocytes expressing GIRK1/2 without GPR37 were unresponsive to HA (Fig. 5B). Comparable dose-response curves were obtained from 30 oocytes.

HA signal transduction

One of the most prominent effects of HA is that it stimulates cells to enter mitosis (Hampe et al., 2000; Kayser et al., 1998; Ulrich et al., 1996). At the G2-mitosis transition, histone H3 is phosphorylated and is, therefore, an excellent marker for mitotic events. HEK-T-REx–GPR37 cells were incubated with and without doxycycline for 24 hours, before HA was added for 1.7 hours. Cells induced with doxycycline to express GPR37 showed an increase over uninduced cells in the percentage of mitotic cells, as visualised with the antibody against phosphorylated histone H3 (Fig. 6A). This suggested a direct role for GPR37 in mediating the action of HA as a mitogen. To monitor HA signalling mediated by GPR37, transiently transfected COS-7 cells and HEK-T-REx–GPR37 cells were subjected to electrophysiological analysis by patch clamping. Treatment of cells with HA led

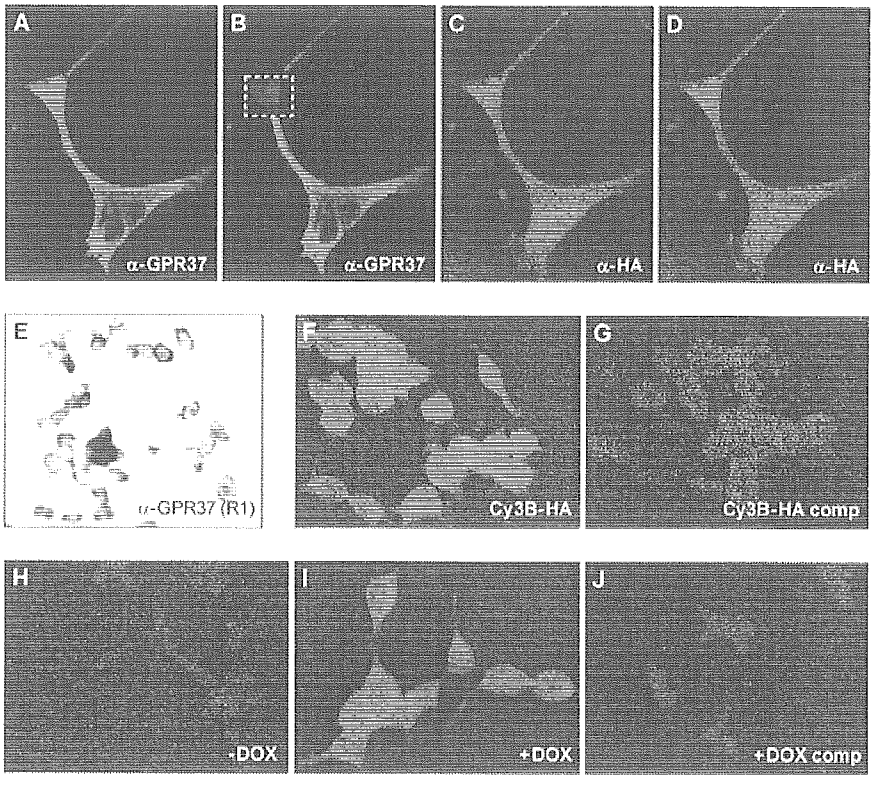

Fig. 3. HA colocalises with and binds to GPR37. (A-D) Interaction of HA and GPR37 analysed by FRET. Shown is a typical example of FRET between HA and an extracellular epitope of GPR37. COS-7 cells transiently transfected with GPR37 were treated with 2 nM HA for 20 minutes on ice to prevent internalisation, followed by incubation for 20 minute on ice with the antiserum against HA (-HA). After fixation with 4% formaldehyde in PBS, cells were immunostained with anti-GPR37 antibody (-GPR37). GPR37 immunoreactivity was visualised with Cy3 (A,B) and that of HA with Alexa Fluor 488 (C,D). (A) The Cy3 signal (GPR37) is shown after excitation at 568 nm. (B) A discrete area was photobleached using intense 568 nm laser. The Alexa Fluor 488 signal (HA) after excitation at 488 nm is shown before (C) and after (D) photobleaching. In this example, the Alexa Fluor 488 signal was increased by 18%. (E-G) The neuroblastoma cell line NH15-CA2 was used as a positive control to show specific Cy3B-HA binding to endogenous HA receptors. (E) NH15-CA2 cells endogenously express GPR37, as visualised with anti-GPR37(R1) antibody [-GPR37(R1)]. (F,G) Binding is optimal at 150 nM of Cy3B-HA after incubation for 10 minutes at 37°C (Cy3B-HA) and is inhibited by pretreatment for 50 minutes at 37°C with 100 nM unlabelled, monomerised HA (Cy3B-HA comp). (H-J) HEK-T-REx–GPR37 cells bound Cy3B-HA only after GPR37 induction with doxycycline (±DOX), and binding was competed with unlabelled HA (+DOX comp).

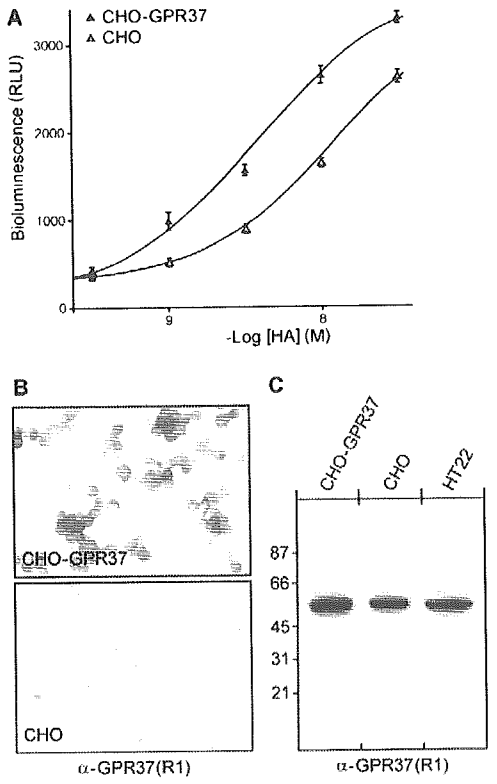

Fig. 4. HA stimulates Ca^{2+} mobilisation in CHO-K1 cells stably transfected with GPR37-FLAG, G 16 and apoaequorin. (A) The Ca^{2+}-bioluminescence response was measured at 469 nm and is expressed in relative light units (RLU), from which the medium response was subtracted. Values are given as means ± s.d. CHO-G 16-AEQ cells stably expressing GPR37-FLAG (CHO-GPR37) responded with an EC_{50} value of 3.3 nM; the endogenous response of CHO-G 16-AEQ cells (CHO) resulted in an EC_{50} value of 11 nM. Data show representative results of three independent experiments. (B) CHO-GPR37 (upper panel) and CHO cells (lower panel) reacted with anti-GPR37(R1) antibody [-GPR37(R1)], a polyclonal antiserum produced against the conserved intracellular C-tail. (C) Western blot analysis of membrane fractions confirmed an increased expression of GPR37 in transfected cells. The mouse hippocampal cell line HT22, expressing GPR37 endogenously, was used as a positive control.

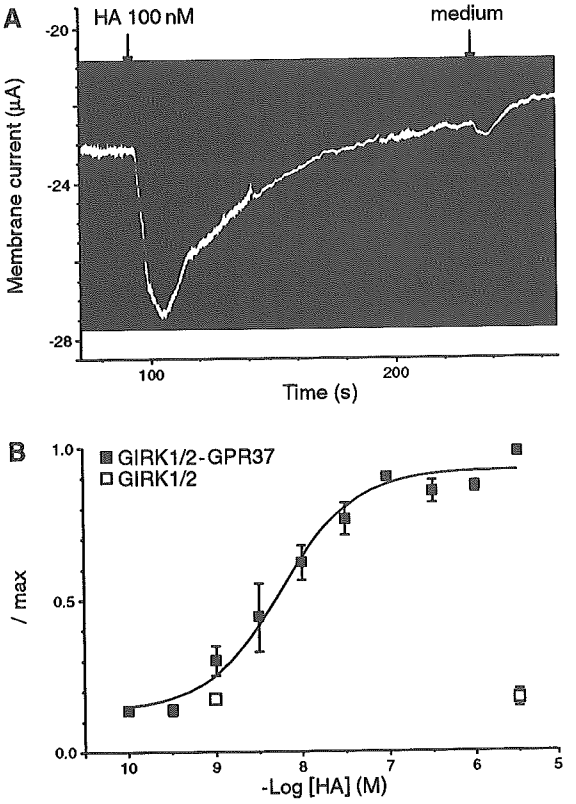

Fig. 5. HA is a high-affinity ligand for GPR37 expressed in frog oocytes. (A) Currents induced by 100 nM HA were recorded from *Xenopus* oocytes injected with cRNAs coding for GPR37 and for GIRK1/2. Stimulation with medium served as control. (B) The current increase was dependent on HA concentration. Dose-response curves for a HA-induced increase in GIRK1/2-mediated inward currents were normalised against maximal currents obtained for each oocyte. Current increases were averaged over four oocytes prepared and injected on the same day. The values represent means ± s.d. Data are representative of several independent experiments.

to an increase in membrane currents (Fig. 6B), which was blocked by La^{3+} and by SKF (Fig. 6B), both of which are known inhibitors of TRP-like Ca^{2+} channels. These Ca^{2+} channels, upon stimulation of receptors with ligands, translocate from an intracellular pool to the plasma membrane, for which activation of phosphoinositide 3-kinase (PI 3-kinase) and Ca^{2+}-dependent calmodulin (CaM) kinase is a prerequisite (Boels et al., 2001). The HA-induced increase in current was prevented by pre-incubating cells with pertussis toxin, wortmannin and KN93 (Fig. 6C), which demonstrates that an inhibitory G protein, PI 3-kinase and CaM-kinase II, respectively, are involved in the HA-GPR37 signalling cascade. A preliminary scheme of HA signalling is shown in Fig. 7.

Discussion

We present evidence that HA is a high-affinity ligand for GPR37. After heterologous expression in frog oocytes and in mammalian cells, EC_{50} values in the low nanomolar range were obtained. Electrophysiological analysis revealed that GPR37 activation by HA involved the same signalling cascade (Fig. 7) as found earlier for the endogenous HA receptor (Boels et al., 2001; Kayser et al., 1998; Ulrich et al., 1996). Interaction with HA resulted in GPR37 internalisation and stimulated entry into mitosis.

HA is bound to a carrier-like molecule both in hydra and in mammals, which improves the half-life and function of HA (Roberge et al., 1984; Schaller et al., 1996). The HA-binding protein HAB was isolated from hydra using HA-affinity chromatography, and later SorLA was discovered as an orthologue of HAB (Hampe et al., 2000). SorLA is a multi-ligand sorting receptor that, in addition to HA, binds glial-cell-derived neurotrophic factor (GDNF), PDGF and apolipoprotein E (ApoE) (Gliemann et al., 2004; Taira et al., 2001; Westergaard et al., 2004). HAB and SorLA are type I

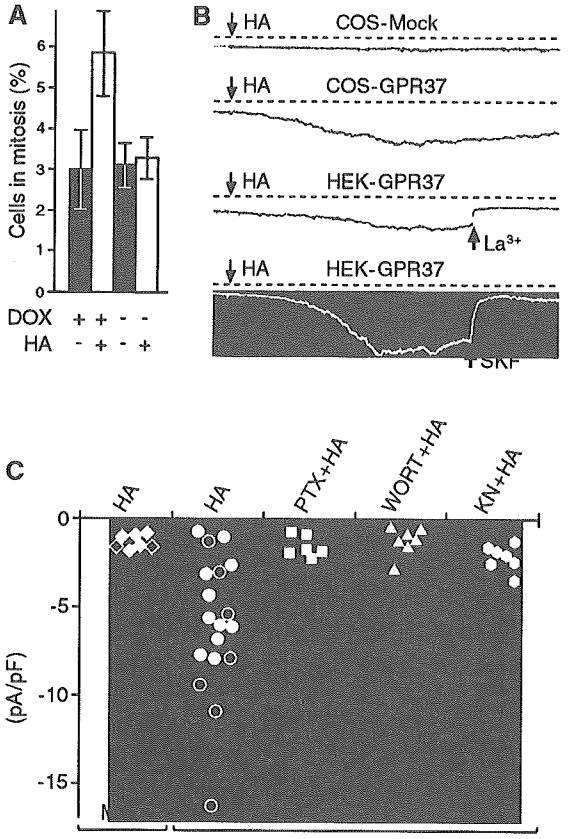

Fig. 6. GPR37 mediates HA signalling to stimulate mitosis. (A) HEK-T-REx–GPR37 cells were treated with and without doxycycline for 24 hours. Incubation with 2 nM HA for 1.7 hours led to an increase of cells in mitosis after induction of GPR37 expression. Immunostaining of cells with anti-phospho-histone H3 (1:1000) was used to determine cells in mitosis. 6 350 cells were counted, and the percentage of stained mitotic cells is given as means ± s.d. (B) Membrane currents were measured in the perforated patch configuration at a holding potential of –80 mV. Treatment with 1 nM HA induced an increase in membrane currents in COS-7 cells transiently expressing GPR37 (COS-GPR37), but not in mock-injected cells (COS-Mock). Membrane currents activated by HA in HEK-T-REx–GPR37 cells were blocked by application of 1 mM La^{3+} or 10 M SKF. (C) Membrane-current densities were recorded from mock- and GPR37-transfected COS-7 cells. HA signal transduction was inhibited by pretreating cells for 2-3 hours with 200 ng ml^{-1} pertussis toxin (PTX), for 30-60 minutes with 100 nM wortmannin (WORT), or 30 M KN93 (KN). Each symbol represents one cell measured in the whole-cell (filled symbols) or the perforated patch (open symbols) configuration

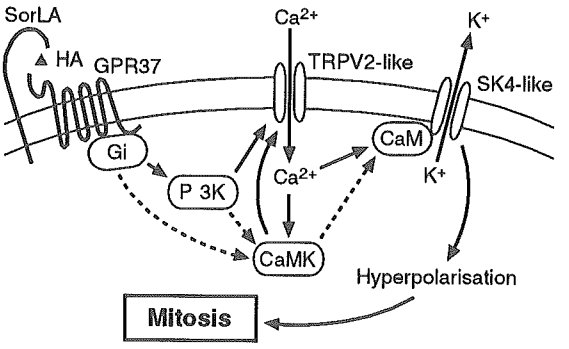

Fig. 7. Scheme of the signalling pathway from HA through GPR37 to stimulate mitosis. After binding of HA to GPR37 with or without help of the coreceptor SorLA, a pertussis-toxin-sensitive inhibitory G protein (Gi) is activated, which interacts through the phosphoinositide 3-kinase (PI3K) and the calcium-calmodulin dependent kinase II (CaMK) with a Ca^{2+} channel of the transient receptor potential family (TRPV2-like). The resulting Ca^{2+} influx activates a Ca^{2+}-dependent K^+ channel of the small and intermediate conductance family (SK4-like), leading to hyperpolarisation, which is a prerequisite for cells to enter mitosis. Dashed lines indicate hypothetical pathways.

transmembrane receptors with a large extracellular domain that can be shed by metalloprotease cleavage (Hampe et al., 2000). This represents an ideal mechanism to regulate the range of action of a morphogen like HA. GPR37 contains a relatively large extracellular domain, which is unusual for a peptide receptor. The notion that SorLA interacts with this domain of GPR37 as co-receptor to enhance HA binding (Hampe et al., 2000) is plausible and outlined in Fig. 7.

GPCRs play key physiological roles, and their dysfunction is implicated in several diseases. This might be reflected by the fact that about half of the current drugs, and certainly more in the future, are targeted to these receptors. GPR37 is of special interest for pharmacology, since it was shown to contribute to Parkinson's disease. GPR37 was characterised as a substrate for the E3 ubiquitin ligase parkin (Imai et al., 2001). Ubiquitylation marks proteins for degradation. Parkin mutations have been shown to be causative for neurodegeneration in Parkinson's disease, where dopaminergic neurons of the substantia nigra are especially affected (Imai et al., 2001; Yang et al., 2003). We found that overexpression of GPR37 resulted in complexes of molecular masses 250 kDa. Aggregated GPR37 did not translocate to the cell surface, as shown by cell-surface biotinylation experiments, and most probably led to preferential cell death of transfected cells. We could express GPR37 successfully in frog oocytes and in mammalian cells after stable integration into the chromosome. Since frog oocytes are cultured at room temperature, more time for proper folding may have been advantageous for GPR37 expression. Similarly, lower levels of GPR37 transcripts by stable expression may have caused less stress for the cells. The fact that insoluble GPR37 was enriched in brains of patients with juvenile Parkinson's disease (Imai et al., 2001) and its presence in Lewy bodies (Murakami et al., 2004) supports the notion that GPR37 misfolding contributes to neuronal cell death (Imai et al., 2003). This might be confirmed by the recent finding that GPR37-knockout mice showed altered dopaminergic signalling and were resistant to the neurotoxin 1-methyl-4-phenyl-1,2,3,6-tetrahydropyridine (MPTP), which preferentially kills dopaminergic neurons (Marazziti et al., 2004). As SorLA was found to be downregulated in the brains of patients with Alzheimer's disease (Scherzer et al., 2004), it is intriguing to speculate that a connection exists between SorLA, GPR37 and HA to improve neuronal cell survival.

Materials and Methods

Monomerisation of HA and synthesis of Cy3B-labelled HA

HA was from Bachem AG. Monomerisation was achieved by heating a 10 M solution of HA in 0.1 N HCl for 5 minutes to 95°C. After neutralisation with NaOH to pH 7.0, samples were stored frozen at –20°C and used 2-3 times only (Bodenmuller et al., 1986). For labelling Cy3B, 150 nmoles of monomerised HA were lyophilised and dissolved in 100 l dimethylformamide containing 0.2% *N*-methylmorpholine. Cy3B-mono-*N*-hydroxysuccinimide (NHS) ester (Amersham Biosciences) was dissolved in the same buffer (0.5 mg in 50 l) and incubated with HA overnight in the dark. The Cy3B-labelled HA was purified by C18 reverse-phase HPLC, yielding approximately 30-40 nmoles of Cy3B-labelled HA.

Molecular biology

Human GPR37 cDNA was inserted into pcDNA 3.1 (+) and into pcDNA3-FLAG-His6C as described earlier (Imai et al., 2001). GPR37 and GPR37-FLAG were subcloned into the dual-function vector pXOON, a kind gift from T. Jespersen, optimised for expression both in frog oocytes and in mammalian cells (Jespersen et al., 2002). GPR37-FLAG was introduced into CHO-K1 cells stably expressing G 16 and apoaequorin (CHO-G 16-AEQ) (Stables et al., 1997) with the vector pIRES-P, a kind gift from S. Hobbs (Hobbs et al., 1998). Stable integration was monitored by immunostaining with antibodies against FLAG (Sigma-Aldrich). For inducible expression, GPR37 was transfected into HEK-293 cells using the Flp-In T-REx system of Invitrogen (Karlsruhe, Germany). The concatemeric construct between GIRK1 and GIRK2 (GIRK1/2) was kindly provided by A. Karschin (Wischmeyer et al., 1997). All constructs were confirmed by sequencing.

Expression of GPR37 in *Xenopus laevis* oocytes and electrophysiology

For functional expression in frog oocytes, the GPR37 cRNA was transcribed in vitro with T7 polymerase from the *Xba*I-linearised pXOON-GPR37-FLAG vector and co-injected at a ratio of 5:1 with cRNA of the concatemeric GIRK1/2 construct transcribed from the *Nhe*I-linearised plasmid. For recordings, oocytes were superfused with ND-96 medium (96 mM NaCl, 2 mM KCl, 1.8 mM $CaCl_2$, 1 mM $MgCl_2$, 5 mM Hepes, pH 7.5). Two-electrode voltage-clamp recordings were performed with electrodes pulled to a tip resistance of 0.5-2.0 M . A Gene Clamp 500B amplifier (Axon Instruments), pClamp9 (Axon Instruments) and Origin (Microcal Software) served for data acquisition and analysis. Whole cells were clamped at –100 mV. For agonist measurements, the medium was changed to high K^+ (ND-96 with 96 mM KCl, 2 mM NaCl). After the initial inward current had reached a plateau, agonists were applied in high K^+ medium. Agonist treatment was terminated by wash-out with low K^+ to control intactness of the oocyte membrane. All recordings were performed at room temperature.

Cell culture, transfection and immunostaining

NH15-CA2, HT22 and COS-7 cells were cultured in DMEM supplemented with 10% fetal calf serum (FCS), HEK-T-REx-GPR37 cells with 10% newborn calf serum (tetracycline-free) and CHO-K1 cells in DMEM-F12 with 5% FCS. For routine culture, 100 U ml^{-1} penicillin, 100 g ml^{-1} streptomycin and 10 mM Hepes, pH 7, were added to these media. CHO-G 16-AEQ cells stably expressing GPR37 required the addition of 750 g ml^{-1} geneticin, 200 g ml^{-1} hygromycin and 5 g ml^{-1} puromycin. HEK-T-REx-GPR37 cells were induced to express GPR37 by incubation in 1 g ml^{-1} doxycycline. Lipofectamine 2000 (Invitrogen), Fugene 6 (Roche Diagnostics), or electroporation were used for transfection. To assay ligands, cells were transferred overnight into serum-free defined medium consisting of the respective basal media to which 5 g ml^{-1} insulin, 30 g ml^{-1} transferrin, 20 M ethanolamine, 30 nM sodium selenite, 1 M sodium pyruvate, 1% non-essential amino acids and 2 mM glutamine were added.

For immunocytochemistry, cells were fixed either with 4% formaldehyde in PBS for 30 minutes at room temperature or with ice-cold 1% acetic acid in ethanol for 5 minutes. After washing with 0.1% Triton X-100 and pre-absorption with 1% bovine serum albumin, first and second antibodies were applied. For cell-surface staining, living cells were incubated with ligand and/or antisera for 20-30 minutes on ice, washed, fixed and visualised as indicated. No Triton X-100 was added to prevent permeabilisation. For western blotting, cells were harvested by treatment with 2 mM EDTA in PBS for 10 minutes, collected by centrifugation, and ultrasonicated for 20 seconds in Tris-HCl buffer, pH 7.4, containing 2 mM EDTA and a protease-inhibitor cocktail (Roche Diagnostics). After centrifugation at 100,000 *g*, the membrane pellets were dissolved in sample buffer and separated by SDS-PAGE. The monoclonal mouse anti-GPR37 antibody, recognising an extracellular domain of recombinant human GPR37, was used at a dilution of 1:400, the polyclonal rabbit antisera against the intracellular C-terminal domain of GPR37, anti-GPR37(R1) and anti-GPR37(R2), were diluted 1:1000 and 1:2000, respectively. All GPR37-specific antibodies were produced in the laboratory of Takahashi and have been described previously (Imai et al., 2001). The antibody against FLAG (M2) was from Sigma-Aldrich and that against phospho-histone H3 from Biomol. Cy2 or Cy3 secondary antibodies were used for confocal analysis, and alkaline phosphatase- or peroxidase-conjugated secondary antibodies were used for light microscopy and western blotting. Western blots were visualised by ECL. Biotinylated proteins were detected with an avidin-peroxidase conjugate (Bio-Rad).

FRET analysis

For fluorescence resonance energy transfer (FRET) experiments, HA was reacted with the highly specific HA antiserum 102.8, which binds to HA in the picomolar range and was described earlier (Schaller et al., 1984). It was used at a dilution of 1:3000 and visualised with Alexa Fluor 488 goat anti-rabbit as donor (Invitrogen). GPR37 was detected with anti-GPR37 antibody and visualised with Cy3 anti-mouse antibody (Amersham) as acceptor. The energy transfer was detected as increase in donor fluorescence (Alexa Fluor 488) after complete photobleaching of the acceptor molecule (Cy3). Initial images were recorded after excitation at 488 and 568 nm. A discrete area of the sample was illuminated with intense 568 nm light (laser power 100%) for a few minutes to destroy completely the acceptor fluorescence. The cell was then rescanned using excitation at 488 nm. An increase within the photobleached area was used as a measure for the amount of FRET obtained. The efficiency of energy transfer (E) was expressed as E=1-(D1/D2), where D1 is the donor fluorescence before, and D2 after, photobleaching. Data were collected for 4-5 different fields from a single coverslip; 2-3 coverslips were used for each measurement; the experiment was repeated at least three times.

Biotinylation of surface proteins

COS-7 cells were transiently transfected with GPR37-FLAG using the Fugene 6 reagent (Roche Diagnostics). 48 hours after transfection, cells were washed 2 with PBS and biotinylated for 30 minutes at room temperature with 1 mM S-NHS-biotin (Perbio Science). The reaction was stopped by addition of 0.5 M Tris-HCl, pH 7.5, for 5 minutes at room temperature, and the cells were washed with PBS to remove free biotin. Cell lysates were prepared in a buffer consisting of 5 mM EDTA, 10 mM Tris-HCl, pH 7.4, and protease-inhibitor cocktail. Samples were ultrasonicated for 20 seconds and centrifuged at 100,000 *g* for 30 minutes. Pellets were solubilised in buffer containing 1% Triton X-100, 0.5% NP40, 150 mM NaCl, 7 mM EDTA, 1 mM EGTA, 10 mM Tris-HCl, pH 7.4, and protease-inhibitor cocktail for 30 minutes on ice, followed by centrifugation at 16,000 *g* for 15 minutes at 4°C. The supernatant was used for immunoprecipitation.

Immunoprecipitation with anti-FLAG M2-agarose

Since high concentrations of NP40 inhibited binding to FLAG-agarose, the supernatant from the NP40-solubilised and biotinylated COS-7 cells was diluted fivefold with TBS (150 mM NaCl, 50 mM Tris-HCl, pH 7.4) to reduce the NP40 concentration to 0.1%. Samples were incubated with 100 l anti-FLAG M2-agarose (Sigma-Aldrich) overnight at 4°C and then centrifuged at 1500 *g* for 5 minutes at 4°C. Pellets were resuspended in 1 ml TBS and centrifuged again at 16,000 *g* for 2 minutes at 4°C. After washing with TBS, pellets were dissolved in 50 l sample buffer and subjected to western blotting.

Electrophysiology with mammalian cells

For electrical recordings, COS-7 cells were microinjected with 50 ng l^{-1} GPR37-pcDNA3 and 5 ng l^{-1} EGFP-N1-pcDNA3, the latter being used to facilitate detection of successfully transfected cells. Membrane currents were recorded in the whole-cell configuration of the patch-clamp technique (Hamill et al., 1981) or the perforated-patch configuration with nystatin (Horn and Marty, 1988). An EPC9 patch-clamp amplifier was used in conjunction with the PULSE-stimulation and data-acquisition software (HEKA Elektronik). The patch electrodes were made from 1.5 mm diameter borosilicate glass capillaries with resistances of 2.5-4 M . Data were low-pass filtered at 3 kHz and compensated for both fast and slow capacity transients. Series resistance was compensated by 75-90%. All experiments were performed at room temperature (22-25°C). The pipette solution contained 140 mM KCl, 2 mM $MgCl_2$, 1 mM $CaCl_2$, 2.5 mM EGTA, 10 mM HEPES and had a calculated free Ca^{2+} concentration of 66 nM. The pH was adjusted to 7.3 with KOH. The standard external solutions contained 140 mM NaCl, 2 mM $MgCl_2$, 2 mM $CaCl_2$, 5 mM KCl, 10 mM HEPES and 10 mM glucose, buffered to pH 7.3 with NaOH. Nystatin was dissolved in dimethyl sulfoxide (DMSO). Its final concentration in the standard pipette solution was 0.2 mg ml^{-1}. All chemicals for electrophysiology were purchased from Sigma-Aldrich.

Statistical analysis

The results are expressed as means of 3-6 determinations ± s.d. Curve fittings were performed with the Prism program (GraphPad). Each experiment was repeated at least three times.

We thank T. Jespersen for providing the vector pXOON, S. Hobbs for pIRES-P, A. Karschin for the concatemeric GIRK1/2 construct, J. Stables for the CHO-G 16-AEQ cell line and S. Hempel for help with the figures.

References

Bodenmuller, H. and Schaller, H. C. (1981). Conserved amino acid sequence of a neuropeptide, the head activator, from coelenterates to humans. *Nature* **293**, 579-580.

Bodenmuller, H., Schilling, E., Zachmann, B. and Schaller, H. C. (1986). The neuropeptide head activator loses its biological activity by dimerization. *EMBO J.* **5**, 1825-1829.

Boels, K. and Schaller, H. C. (2003). Identification and characterisation of GPR100 as a novel human G-protein-coupled bradykinin receptor. *Br. J. Pharmacol.* **140**, 932-938.

Boels, K., Glassmeier, G., Herrmann, D., Riedel, I. B., Hampe, W., Kojima, I., Schwarz, J. R. and Schaller, H. C. (2001). The neuropeptide head activator induces activation and translocation of the growth-factor-regulated Ca^{2+}-permeable channel GRC. *J. Cell Sci.* **114**, 3599-3606.

Frederiksson, R., Lagerström, M. C., Lundin, L. G. and Schiöth, H. B. (2003). The G-protein-coupled receptors in the human genome form five main families. Phylogenetic analysis, paralogon groups, and fingerprints. *Mol. Pharmacol.* **63**, 1256-1272.

Gliemann, J., Hermey, G., Nykjær, A., Petersen, C. M., Jacobsen, C. and Andreasen, P. A. (2004). The mosaic receptor sorLA/LR11 binds components of the plasminogen-activating system and platelet-derived growth factor-BB similarly to LRP1 (low-density lipoprotein receptor-related protein), but mediates slow internalization of bound ligand. *Biochem. J.* **38**, 203-212.

Hamill, O. P., Marty, A., Neher, E., Sakmann, B. and Sigworth, F. J. (1981). Improved patch-clamp techniques for high-resolution current recording from cells and cell-free membrane patches. *Pflügers Arch.* **391**, 85-100.

Hampe, W., Riedel, I. B., Lintzel, J., Bader, C. O., Franke, I. and Schaller, H. C. (2000). Ectodomain shedding, translocation and synthesis of SorLA are stimulated by its ligand head activator. *J. Cell Sci.* **113**, 4475-4485.

Hobbs, S., Jitrapakdee, S. and Wallace, J. C. (1998). Development of a bicistronic vector driven by the human polypeptide chain elongation factor 1Alpha promoter for creation of stable mammalian cell lines that express very high levels of recombinant proteins. *Biochem. Biophys. Res. Commun.* **251**, 368-372.

Horn, R. and Marty, A. (1988). Muscarinic activation of ionic currents measured by a new whole-cell recording method. *J. Gen. Physiol.* **92**, 145-159.

Ignatov, A., Lintzel, J., Hermans-Borgmeyer, I., Kreienkamp, H. J., Joost, P., Thomsen, S., Methner, A. and Schaller, H. C. (2003a). Role of the G-protein-coupled receptor GPR12 as high-affinity receptor for sphingosylphosphorylcholine and its expression and function in brain development. *J. Neurosci.* **23**, 907-914.

Ignatov, A., Lintzel, J., Kreienkamp, H. J. and Schaller, H. C. (2003b). Sphingosine-1-phosphate is a high-affinity ligand for the G protein-coupled receptor GPR6 from mouse and induces intracellular Ca^{2+} release by activating the sphingosine-kinase pathway. *Biochem. Biophys. Res. Commun.* **311**, 329-336.

Imai, Y., Soda, M., Inoue, H., Hattori, N., Mizuno, Y. and Takahashi, R. (2001). An unfolded putative transmembrane polypeptide, which can lead to endoplasmic reticulum stress, is a substrate of Parkin. *Cell* **105**, 891-902.

Imai, Y., Soda, M., Murakami, T., Shoji, M. and Abe, K. (2003). A product of the human gene adjacent to *parkin* is a component of Lewy bodies and suppresses Pael receptor-induced cell death. *J. Biol. Chem.* **278**, 51901-51910.

Jespersen, T., Grunnet, M., Angelo, K., Klaerke, D. A. and Olesen, S. P. (2002). Dual-function vector for protein expression in both mammalian cells and *Xenopus laevis* oocytes. *BioTechniques* **32**, 536-540.

Kanzaki, M., Zhang, Y.-Q., Mashima, H., Li, L., Shibata, H. and Kojima, I. (1999). Translocation of a calcium-permeable cation channel induced by insulin-like growth factor-I. *Nat. Cell Biol.* **40**, 339-344.

Kayser, S. T., Ulrich, H. and Schaller, H. C. (1998). Involvement of a Gardos-type potassium channel in head activator-induced mitosis of BON cells. *Eur. J.Cell Biol.* **76**, 119-124.

Kofuji, P., Davidson, N. and Lester, H. A. (1995). Evidence that neuronal G-protein-gated inwardly rectifying K^+ channels are activated by G subunits and function as heteromultimers. *Proc. Natl. Acad. Sci. USA* **92**, 6542-6546.

Marazziti, D., Golini, E., Gallo, A., Lombardi, M. S., Matteoni, R. and Tocchini-Valentini, G. P. (1997). Cloning of GPR37, a gene located on chromosome 7 encoding a putative G-protein-coupled peptide receptor, from a human frontal brain EST library. *Genomics* **45**, 68-77.

Marazziti, D., Golini, E., Magrelli, A., Matteoni, R. and Tocchini-Valentini, G. P. (2001). Genomic analysis of *GPR37* and related orphan G-protein coupled receptor genes highly expressed in the mammalian brain. *Curr. Genom.* **2**, 253-260.

Marazziti, D., Golini, E., Mandillo, S., Magrelli, A., Witke, W., Matteoni, R. and Tocchini-Valentini, G. P. (2004). Altered dopamine signaling and MPTP resistance in mice lacking the Parkinson's disease-associated GPR37/parkin-associated endothelin-like receptor. *Proc. Natl. Acad. Sci. USA* **101**, 10189-10194.

Ménard, L., Ferguson, S. S. G., Zhang, J., Lin, F.-T., Lefkowitz, R. J., Caron, M. G. and Barak, L. S. (1997). Synergistic regulation of $_2$-adrenergic receptor sequestration: Intracellular complement of -adrenergic receptor kinase and -arrestin determine kinetics of internalization. *Mol. Pharmacol.* **51**, 800-808.

Murakami, T., Shoji, M., Imai, Y., Inoue, H., Kawarabayashi, T., Matsubara, E., Harigaya, Y., Sasaki, A., Takahashi, R. and Abe, K. (2004). Pael-R is accumulated in Lewy bodies of Parkinson's disease. *Ann. Neurol.* **55**, 439-442.

Niemann, S. and Schaller, H. C. (1996). Head activator and the neuroectodermal differentiation of P19 mouse embryonal carcinoma cells. *Neurosci. Lett.* **207**, 49-52.

Roberge, M., Escher, E., Schaller, H. C. and Bodenmuller, H. (1984). The hydra head activator in human blood circulation. Degradation of the synthetic peptide by plasma angiotensin-converting enzyme. *FEBS Lett.* **173**, 307-313.

Schaller, H. C., Bodenmuller, H., Zachmann, B. and Schilling, E. (1984). Enzyme-linked immunosorbent assay for the neuropeptide 'head activator'. *Eur. J. Biochem.* **138**, 365-371.

Schaller, H. C., Hermans-Borgmeyer, I. and Hoffmeister, S. A. H. (1996). Neuronal control of development in hydra. *Int. J. Dev. Biol.* **40**, 339-344.

Scherzer, C. R., Offe, K., Gearing, M., Ress, H. D., Fang, G., Heilman, C. J., Schaller, H. C., Bojo, H., Levey, A. I. and Lah, J. J. (2004). Loss of apolipoprotein E receptor LR11 in Alzheimer disease. *Arch. Neurol.* **61**, 1200-1205.

Stables, J., Green, A., Marshall, F., Fraser, N., Knight, E., Sautel, M., Milligan, G., Lee, M. and Rees, S. (1997). A bioluminescent assay for agonist activity at potentially any G-protein-coupled receptor. *Anal. Biochem.* **252**, 115-126.

Taira, K., Bujo, H., Hirayama, S., Yamazaki, H., Kanaki, T., Takahashi, K., Ishii, I., Miida, T., Schneider, W. J. and Saito, Y. (2001). LR11, a mosaic LDL receptor family member, mediates the uptake of ApoE-rich lipoproteins in vitro. *Arterioscler. Thromb. Vasc. Biol.* **21**, 1501-1506.

Ulrich, H., Tárnok, A. and Schaller, H. C. (1996). Head-activator induced mitosis of NH15-CA2 cells requires calcium influx and hyperpolarization. *J. Physiol. (Paris)* **90**, 85-94.

Westergaard, U. B., Sørensen, E. S., Hermey, G., Nielsen, M. S., Nykjær, A., Kirkegaard, K., Jacobsen, C., Gliemann, J., Madsen, P. and Petersen, C. M. (2004). Functional organization of the sortilin Vps10p domain. *J. Biol. Chem.* **279**, 50221-50229.

Wischmeyer, E., Doring, F., Wischmeyer, E., Spauschus, A., Thomzig, A., Veh, R. and Karschin, A. (1997). Subunit interactions in the assembly of neuronal Kir3.0 inwardly rectifying k+ channels. *Mol. Cell Neurosci.* **9**, 194-206.

Yang, Y., Nishimura, I., Imai, Y., Takahashi, R. and Lu, B. (2003). Parkin suppresses dopaminergic neuron-selective neurotoxicity induced by Pael-R in Drosophila. *Neuron* **37**, 911-924.

Zeng, Z., Su, K., Kyaw, H. and Li, Y. (1997). A novel endothelin receptor type-B-like gene enriched in the brain. *Biochem. Biophys. Res. Commun.* **233**, 559-567.

Regular Article (NBD-05-378-Revised)

Conditional knockout of Mn superoxide dismutase in postnatal motor neurons reveals resistance to mitochondrial generated superoxide radicals

Hidemi Misawa,[a,b,*] Kazuko Nakata,[a] Junko Matsuura,[a] Yasuhiro Moriwaki,[b] Koichiro Kawashima,[b] Takahiko Shimizu,[c] Takuji Shirasawa,[c] and Ryosuke Takahashi[d,e]

[a]Department of Neurology, Tokyo Metropolitan Institute for Neuroscience, 2-6, Musashidai, Fuchu-shi, Tokyo 183-8526, Japan

[b]Department of Pharmacology, Kyoritsu University of Pharmacy, 1-5-30, Shibakoen, Minato-ku, Tokyo 105-8512, Japan

[c]Department of Molecular Gerontology, Tokyo Metropolitan Institute of Gerontology, 35-2, Sakae-cho, Itabashi-ku, Tokyo 173-0015, Japan

[d]Laboratory for Motor System Neurodegeneration, RIKEN Brain Science Institute, 2-1, Hirosawa, Wako-shi, Saitama 351-0198, Japan

[e]Deparment of Neurology, Graduate School of Medicine, Kyoto University, 54, Sho-goin kawaramachi, Sakyo-ku, Kyoto 606-8507, Japan

*Corresponding author. Department of Pharmacology, Kyoritsu University of Pharmacy, 1-5-30, Shibakoen, Minato-ku, Tokyo 105-8512, Japan

Tel. +81-3-5400-2675

Fax. +81-3-5400-2698

E-mail: misawa-hd@kyoritsu-ph.ac.jp (H. Misawa)

Abstract

Mitochondrial dysfunction and oxidative damage are implicated in the pathogenesis of neurodegenerative disease. Mice deficient in the mitochondrial form of superoxide dismutase (SOD2) die during embryonic or early postnatal development, precluding analysis of a pathological role for superoxide in adult tissue. Here we generated postnatal motor neuron-specific SOD2 knockouts by crossing mice with floxed SOD2 alleles to VAChT-Cre transgenic mice in which Cre expression is restricted to postnatal somatomotor neurons. SOD2 immunoreactivity was specifically lost in a subset of somatomotor neurons resulting in enhanced superoxide production. Yet extensive histological examination revealed no signs of oxidative damage in animals up to 1 year after birth. However, disorganization of distal nerve axons following injury was accelerated in SOD2-deficient motor neurons. These data demonstrate that postnatal motor neurons are surprisingly resistant to oxidative damage from mitochondrial-derived superoxide radicals, but that such damage may sensitize axons to disorganization following nerve injury.

Key Words: Motor neurons; Oxidative stress; Mitochondria; Nerve injury; Conditional knockout; SOD2; Amyotrophic lateral sclerosis

Introduction

Oxygen radicals, of which superoxide ($O_2^{\cdot -}$) is the most abundant, are a natural byproduct of oxygen consumption by the respiratory chain in aerobic ATP production. The superoxide dismutases (SODs) are enzymes that catalyze the conversion of $O_2^{\cdot -}$ to hydrogen peroxide and thus help prevent the build up of toxic $O_2^{\cdot -}$ levels. Three SOD isoforms are expressed in mammalian cells: copper/zinc SOD (SOD1) located in the cytoplasm (McCord and Fridovich, 1969), manganese SOD (SOD2) located in the mitochondrial matrix (Weisiger and Fridovich, 1973) and extracellular SOD (SOD3) (Marklund, 1982; Hjalmarsson et al., 1987). A small fraction of SOD1 is also reported to reside in the intermembrane space of mitochondria (Okado-Matsumoto and Fridovich, 2001; Mattiazzi et al., 2002; Okado-Matsumoto and Fridovich, 2002).

Oxidative stress has been implicated in various neurodegenerative diseases including Parkinson's disease, Alzheimer's disease and amyotrophic lateral sclerosis (ALS). Though it remains unclear whether oxidative stress is a major cause or merely a consequence of cellular dysfunction associated with neurodegenerative diseases (Andersen, 2004), an accumulating body of evidence implicates impaired mitochondrial energy production and increased mitochondrial oxidative damage in early pathological events leading to neurodegeneration (Beal, 1996). Mitochondria are both a major source of reactive oxygen species (ROS) production as well as a major target of ROS-induced cellular injury. Thus mitochondrial localized superoxide dismutase (SOD2) is thought to play an important role in cellular defense against oxidative damage by ROS.

Loss of SOD2 results in embryonic or early postnatal lethality that varies with genetic

background. SOD2 knockout mice on a CD-1 background die either in utero or within 24 hours after birth from severe dilated cardiomyopathy (Li et al., 1995). Similarly, C57BL/6 SOD2 knockout mice die at late embryonic or early neonatal stages from dilated cardiomyopathy (Huang et al., 2001; Ikegami et al., 2002). On a mixed C57BL/6 and 129/Sv background, SOD2 mutant mice survive for up to 18 days, develop a milder-form of dilated cardiomyopathy and display a neurological phenotype (Lebovitz et al., 1996). In contrast, DBA/2J (D2) SOD2 mutant mice do not develop cardiomyopathy but instead develop severe metabolic acidosis and survive an average of 8 days (Huang et al., 2001). This phenotypic variation suggests that sensitivities to SOD2 deficiency are highly dependent on genetic modifiers that differ across strain and cell type.

Motor neurons are believed to be particularly susceptible to oxidative damage given the high metabolic requirement to sustain a large cell size and long axonal processes. Although motor neurons in cell culture are vulnerable to cell death mediated via calcium influx after exposure to glutamate, it is unclear how motor neurons respond to the overproduction of mitochondrial-derived ROS in vivo. To circumvent the early lethality of SOD2 knockout mice, we used a conditional gene deletion approach in which mice with floxed SOD2 genes (Ikegami et al., 2002) were mated with VAChT-Cre mice (Misawa et al., 2003) that express Cre recombinase in approximately 50 % of postnatal somatic motor neurons. Here we report that conditional loss of SOD2 in postnatal motor neurons results in elevated mitochondrial oxidative stress that fails to triggers signs of neurodegeneration under non-pathological conditions. In contrast, nerve axotomy revealed accelerated nerve disorganization, suggesting that adult motor neurons have relative resistance to mitochondrial-generated

superoxide radicals unless stressed.

Materials and Methods

Mice

C57BL/6 mice carrying the VAChT-Cre transgene (VAChT-Cre.Fast and VAChT-Cre.Slow) have been described previously (Misawa et al., 2003). C57BL/6 mice with floxed SOD2 alleles have been described elsewhere (Ikegami et al., 2002). Localization of the VAChT-Cre transgene in the VAChT-Cre.Slow mouse line to chromosome 4 was determined by FISH analysis (data not shown), and VAChT-Cre.Slow mice were used to direct motor neuron-specific Cre expression in this study. Homozygous floxed SOD2 mice (lox/lox) were crossed with VAChT-Cre.Slow heterozygote animals. The resulting double heterozygote animals ($SOD2^{lox/+}$;$Cre^{slow/-}$) were selected and mated with homozygote floxed SOD2 mice. All animals were genotyped for SOD2 allele (Ikegami et al., 2002) and the Cre trensgene (Misawa et al., 2003) using tail DNA as described previously. Motor performance was analyzed using a rota-rod treadmill (MK-600; Muromachi Kikai, Tokyo, Japan) at 28 rpm. Grip strength was measured using a Grip Strength Meter for Mouse (Model 57106; Stoelting, Wood Dale, IL). All animal protocols were approved by the Tokyo Metropolitan Institute for Neuroscience Institutional Animal Care and Use Committee.